nature cell biology

Endothelial cells dynamically compete for the tip cell position during angiogenic sprouting

Lars Jakobsson[1,2], Claudio A. Franco[1], Katie Bentley[1], Russell T. Collins[1], Bas Ponsioen[3], Irene M. Aspalter[1], Ian Rosewell[4], Marta Busse[1], Gavin Thurston[5], Alexander Medvinsky[6], Stefan Schulte-Merker[3] and Holger Gerhardt[1,7].

Sprouting angiogenesis requires the coordinated behaviour of endothelial cells, regulated by Notch and vascular endothelial growth factor receptor (VEGFR) signalling. Here, we use computational modelling and genetic mosaic sprouting assays *in vitro* and *in vivo* to investigate the regulation and dynamics of endothelial cells during tip cell selection. We find that endothelial cells compete for the tip cell position through relative levels of *Vegfr1* and *Vegfr2*, demonstrating a biological role for differential *Vegfr* regulation in individual endothelial cells. Differential *Vegfr* levels affect tip selection only in the presence of a functional Notch system by modulating the expression of the ligand Dll4. Time-lapse microscopy imaging of mosaic sprouts identifies dynamic position shuffling of tip and stalk cells *in vitro* and *in vivo*, indicating that the VEGFR–Dll4–Notch signalling circuit is constantly re-evaluated as cells meet new neighbours. The regular exchange of the leading tip cell raises novel implications for the concept of guided angiogenic sprouting.

Competition between cells to occupy a certain position or to acquire a certain phenotype is involved in various aspects of organogenesis. Cellular competition, first described in the *Drosophila melanogaster* wing, notably also occurs in *Drosophila* tracheal sprouting[1]. Sprouting of *Drosophila* trachea and vertebrate blood vessels both involve the selection of a leading tip cell and following stalk cells[2,3,4,5], but whether cell competition is important in vertebrate sprouting angiogenesis remains unknown.

Endothelial tip cells are induced and guided by an extracellular gradient of vascular endothelial growth factor (VEGF) -A[2,6]. Endothelial cells express three different VEGF receptors (VEGFR)[7]. The tyrosine-kinase activity of VEGFR2 regulates most of the endothelial cell responses to VEGF-A, including induction of tip cell filopodia and endothelial cell migration, proliferation, survival and vascular permeability[7]. VEGFR1 is a high-affinity receptor for VEGF-A, but its weak kinase activity is dispensable for vascular morphogenesis *in vivo*[8,9]. VEGFR1 deficiency leads to severe vessel overgrowth and embryonic lethality[10], probably caused by the loss of VEGFR1 modulating VEGF-A signalling through VEGFR2 (ref. 11). Animals lacking one allele of either *Vegfr1* or *Vegfr2* are viable with no overt vascular phenotypes, whereas deletion of just one allele of the ligand VEGF-A is embryonic lethal[12,13].

The selection of tip- and stalk-cells depends on delta-like 4 (Dll4)–Notch signalling; tip cells have higher levels of Dll4, compared with stalk cells, which are subject to higher levels of Notch signalling[14,15,16,17,18]. Notch signalling influences the level of VEGFRs[19,20,21], suggesting that relative differences in VEGFR levels between adjacent cells may explain how Notch signalling limits sprouting[22]. In turn, VEGFR activity affects expression of the Notch ligand Dll4[23,24], implying that the two pathways integrate in an intercellular feedback loop (Fig. 1a).

A computational model indicated that such a VEGF–VEGFR–Dll4–Notch–VEGFR feedback loop is sufficient to pattern endothelial cells stably into tip and stalk cells, under adequate VEGF-A stimulation [25]. How differential VEGFR levels between endothelial cells affect tip-cell selection and dynamic endothelial behaviour, whether the selection remains stable during sprouting, and whether endothelial cells compete for the tip position is experimentally unexplored.

Using computational modelling in conjunction with genetic mosaic-sprouting assays *in vivo* and *in vitro*, we find that endothelial cells dynamically compete with each other for the tip cell position. Cells with higher *Vegfr2* and lower *Vegfr1* levels stand a better chance to take and maintain the leading position. VEGFR levels have a marked effect upstream of Notch in the selection process by regulating Dll4 levels.

[1]Vascular Biology Laboratory, London Research Institute, Cancer Research UK, 44 Lincoln's Inn Fields, London, WC2A 3PX, UK. [2]Current address: Vascular Biology, Department of Medical Biochemistry and Biophysics, Karolinska Institutet, Scheeles Väg 2, SE171 77 Stockholm, Sweden. [3]Hubrecht Institute, Uppsalalaan 8, 3584 CT Utrecht, Netherlands. [4]Transgenic Services, London Research Institute, Cancer Research UK, Clare Hall Laboratories, Blanche Lane, South Mimms, Potters Bar, Hertfordshire, EN6 3LD, UK. [5]Regeneron Pharmaceuticals, 777 Old Saw Mill River Road, Tarrytown, NY 10591, USA. [6]MRC, Centre for Regenerative Medicine, Chancellor's Building, 49 Little France Crescent, Edinburgh, EH16 4SB, UK. [7]Independent consultant for: Vascular Patterning Laboratory, Vesalius Research Center, Campus Gasthuisberg, O&N1, Herestraat 49-B912, B-3000 Leuven, Belgium.
Correspondence should be addressed to H.G. (e-mail: holger.gerhardt@cancer.org.uk)

Received 18 January 2010; accepted 06 September 2010; published online 26 September 2010; DOI: 10.1038/ncb2103

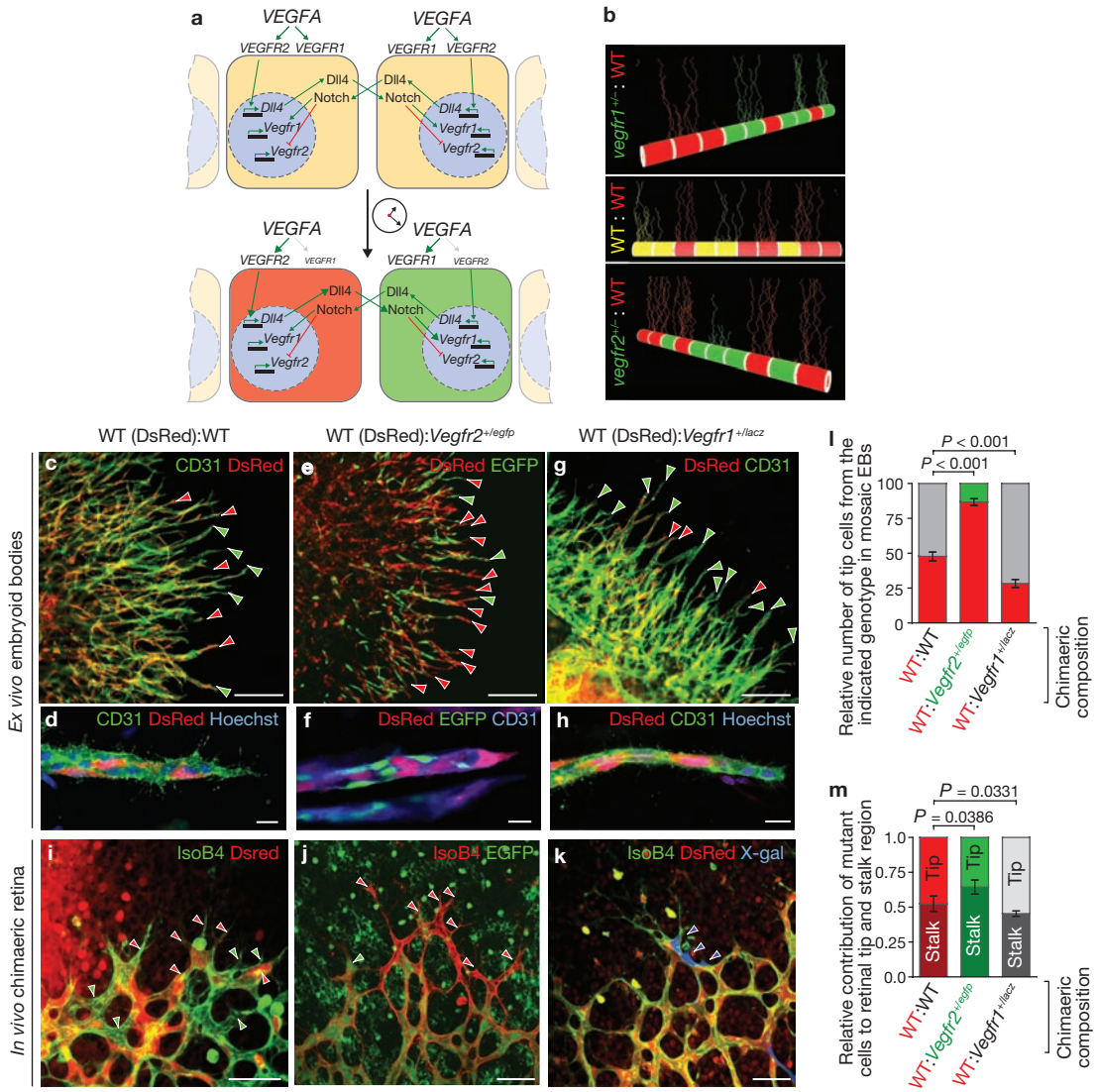

Figure 1 VEGFR levels in mosaic-tip-cell selection *in silico, in vitro* and *in vivo*. (**a**) Schematic representation of how regulatory pathways composed of VEGFRs, Dll4 and Notch1 allow cells to acquire tip (red) or stalk (green) cell phenotype. (**b**) Representative images from *in silico* modelling of tip cell and stalk cell selection in chimaeric vessels comprised of 1:1 mixes of the indicated genotypes. (**c**, **d**) The sprouting vasculature (green) of a chimaeric embryoid body composed of two different wild-type strains, immunolabelled with antibodies specific to CD31. One strain expresses DsRed (tip cells indicated by red arrowheads), the other does not (tip cells indicated by green arrowheads). (**e**, **f**) A chimaeric embryoid body of wild-type (red) and *Vegfr2* heterozygote cells (*Vegfr2*$^{+/egfp}$, green) mixed in a 1:1 ratio. Wild-type tip cells are indicated by red arrowheads, *Vegfr2*$^{+/egfp}$ tip cells are indicated by green arrowheads. (**g**, **h**) A chimaeric embryoid body of wild-type cells (red; tip cells are indicated by red arrowheads) and *Vegfr1* heterozygote cells (tip cells are indicated by green arrrowheads), mixed in a 1:1 ratio. (**i**) Representative image of a retina from a wild-type host (green cells; green arrowheads) injected with wild-type embryonic stem cells expressing DsRed (red cells; indicated by red arrowheads). (**j**) Representative image of a retina from a wild-type host expressing DsRed (red cells; red arrowheads) and injected with *Vegfr*$^{+/egfp}$ embryonic stem cells (green cells; green arrowhead). (**k**) Representative image of a retina from a wild-type host (expressing DsRed) injected with *Vegfr1*$^{+/LacZ}$ embryonic stem cells (indicated by blue arrowheads) and incubated with X-gal (5-bromo-4-chloro-3-indolyl-β-D-galactoside). All retina were assayed 5.5 days postnatal and stained with isolectin B4 conjugated to a fluorophore. (**l**) Quantification of tip cells with the indicated genotype in chimaeric embryoid bodies. Number of counted tips per condition: 630–708 (*n* embryoid bodies per condition = 6, WT:WT; 11, WT:*vegfr2*$^{+/gfp}$; 9, WT:*vegfr1*$^{+/lacz}$). Values represent means ± s.e.m. (**m**) Quantification of the contribution of respective genotypes to the tip versus stalk region in chimaeric mice (see Supplementary Information, Fig. 4 for details). Values represent means ± s.e.m. WT:WT ($n = 5$), *Vegfr2*$^{+/egfp}$:WT ($n = 10$), *Vegfr1*$^{+/lacz}$:WT ($n = 8$), where *n* is the number of coupled sectors analysed. Scale bars: **c**, **e**, **g**, 200 μm; **d**, **f**, **h**, 20 μm; **i**–**k**, 50 μm.

Live-cell imaging of sprouting angiogenesis *in vivo* and *in vitro* shows that the tip cell is dynamically challenged and replaced by migrating cells from the stalk region. The combination of the VEGF–Notch feedback and dynamic position-shuffling promotes reiterative sprouting and branching and thus robust network formation during angiogenesis.

RESULTS

Differential VEGFR levels affect tip cell selection

To investigate the role of VEGFR levels and the interactions between neighbouring cells in the selection process, we adapted a computation model[25] to allow various combinations of endothelial cells with half the amount of VEGFR1 or VEGFR2 (compared with wild-type cells)

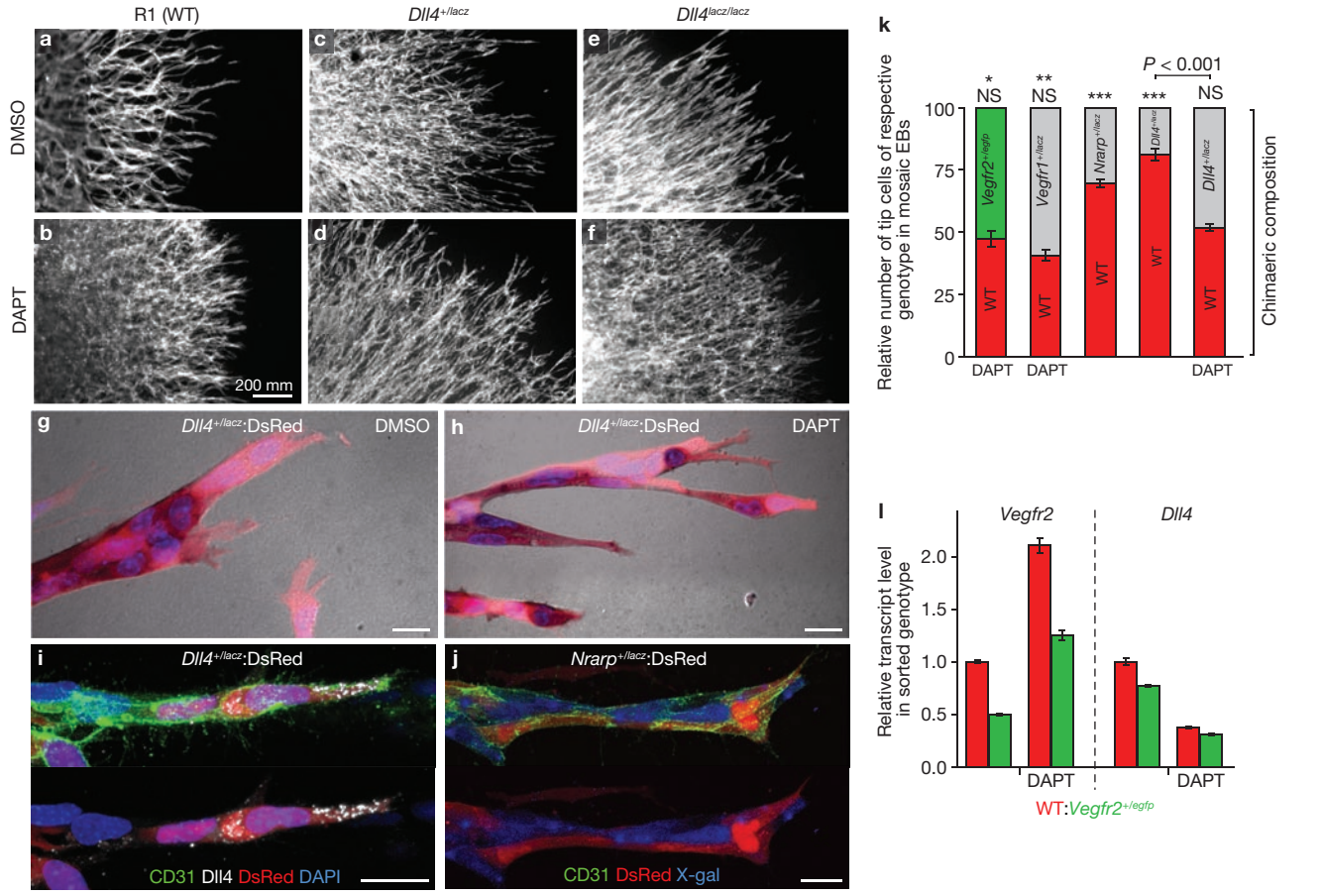

Figure 2 Dll4 and Notch signalling in competition. (**a**–**f**) Representative images of wild-type- (**a**, **b**), *Dll4*$^{+/lacz}$- (**c**, **d**) or *Dll4*$^{lacz/lacz}$- (**e**, **f**) embryoid bodies, untreated (**a**, **c**, **e**) or treated (**b**, **d**, **f**) with the γ-secretase inhibitor, DAPT. After 10 days cells were visualized by immunofluorescence microscopy after treatment with antibodies specific to CD31. (**g**–**i**) Representative images of chimaeric embryoid bodies of wild-type cells expressing DsRed and *Dll4*$^{+/lacz}$ cells, immunostained with antibodies specific to CD31 (**g**, **h,** red; **i**, green) or treated with X-gal (**g**, **h**, dark). Effects of DMSO- and DAPT-treatment are shown in **g** and **h**, respectively. In chimaeric embryoid bodies of *Dll4*$^{+/lacz}$ and wild-type, *Dll4* is expressed by the wild-type leading tip cell (**i**, white). (**j**) Chimaeric sprout comprised of *Nrarp*$^{+/lacz}$- and wild-type- cells. Cells were visualized by treatment with antibodies specific to CD31 (green); *Nrarp*$^{+/lacz}$ cells were identified by treatment with X-gal (indicated as blue cells) and wild-type cells expressed DsRed (red). Scale bars: **a**–**f**, 200 μm; **g**–**j**, 20 μm. (**k**) Quantification of tip cells with the indicated genotype in chimaeric mosaic embryoid bodies. Values represent means ± s.e.m. Number of counted tips per condition: 206–1100. Asterisk indicates that the mean is significantly different from wild-type:*Vegfr2*$^{+/egfp}$ embryoid chimaeras in Figure 1l ($P < 0.001$). Double asterisks indicate mean is significantly different from wild-type:*Vegfr1*$^{+/lacz}$ embryoid chimaeras in Figure 1l ($P = 0.013$). Triple asterisks indicate mean is significantly different from wild-type:wild-type embryoid chimaeras in Figure 1l ($P < 0.003$). WT:*Vegfr2*$^{+/egfp}$ + DAPT ($n = 11$), WT:*Vegfr1*$^{+/lacz}$ + DAPT ($n = 5$), WT:*Nrarp*$^{+/lacz}$ ($n = 3$), WT:*Dll4*$^{+/lacz}$ ($n = 4$), WT:*Dll4*$^{+/lacz}$ + DAPT ($n = 4$). NS; not significantly different from wild-type:wild-type embryoid chimaeras in Figure 1l. (**l**) *Vegfr2* and *Dll4* transcript levels in endothelial cells isolated by FACS from wild-type:*Vegfr2*$^{+/egfp}$ chimaeric cultures, and treated with DAPT, as indicated. Values indicate mean ± s.d. of triplicates in one experiment. Bars separated by the dashed line cannot be compared with respect to absolute expression levels.

to compete with wild-type neighbouring cells for the tip position. Cells heterozygous for *Vegfr2* showed poor contribution to the tip cell population and predominantly became stalk cells in competition with wild-type cells, whereas cells heterozygous for *Vegfr1* dominated the tip cell population. This suggests that the balance of VEGFR2 and VEGFR1 expression in individual endothelial cells affects their potential to become tips cell during sprouting angiogenesis (Fig. 1b).

To test this *in silico* prediction in a cell-based system, we designed a mosaic sprouting assay using mouse (*Mus musculus*) embryonic stem cells (Supplementary Information, Fig. S1). Embryonic stem cells cultured in suspension to form spheroids (embryoid bodies) exhibit robust endothelial differentiation and sprouting angiogenesis when cultured in a solidified collagen I matrix and treated with VEGF-A. This process recapitulates many key elements of angiogenic sprouting *in vivo*[26,27]. Chimaeric embryonic stem cell cultures originating from 1:1 mixtures of two wild-type embryonic stem cell lines; one with ubiquitous expression of the fluorophore DsRed-MST (a variant of the DsRed protein, denoted DsRed) and one non-fluorescent embryonic stem cell line (R1), produced a highly mosaic vasculature (Fig. 1c, d). Confocal microscopy of CD31 labelled endothelial cell-sprouts identified the genotypic origin of the leading tip cells (Fig. 1c, d). Mixtures of different wild-type embryonic stem cells at 1:1 ratio consistently led to an equal (approximately 50%) contribution of each cell population to the leading tip cells, demonstrating that wild-type cells of different genetic background and fluorescent-marker expression had equal potential to acquire the leading tip position (Fig. 1l).

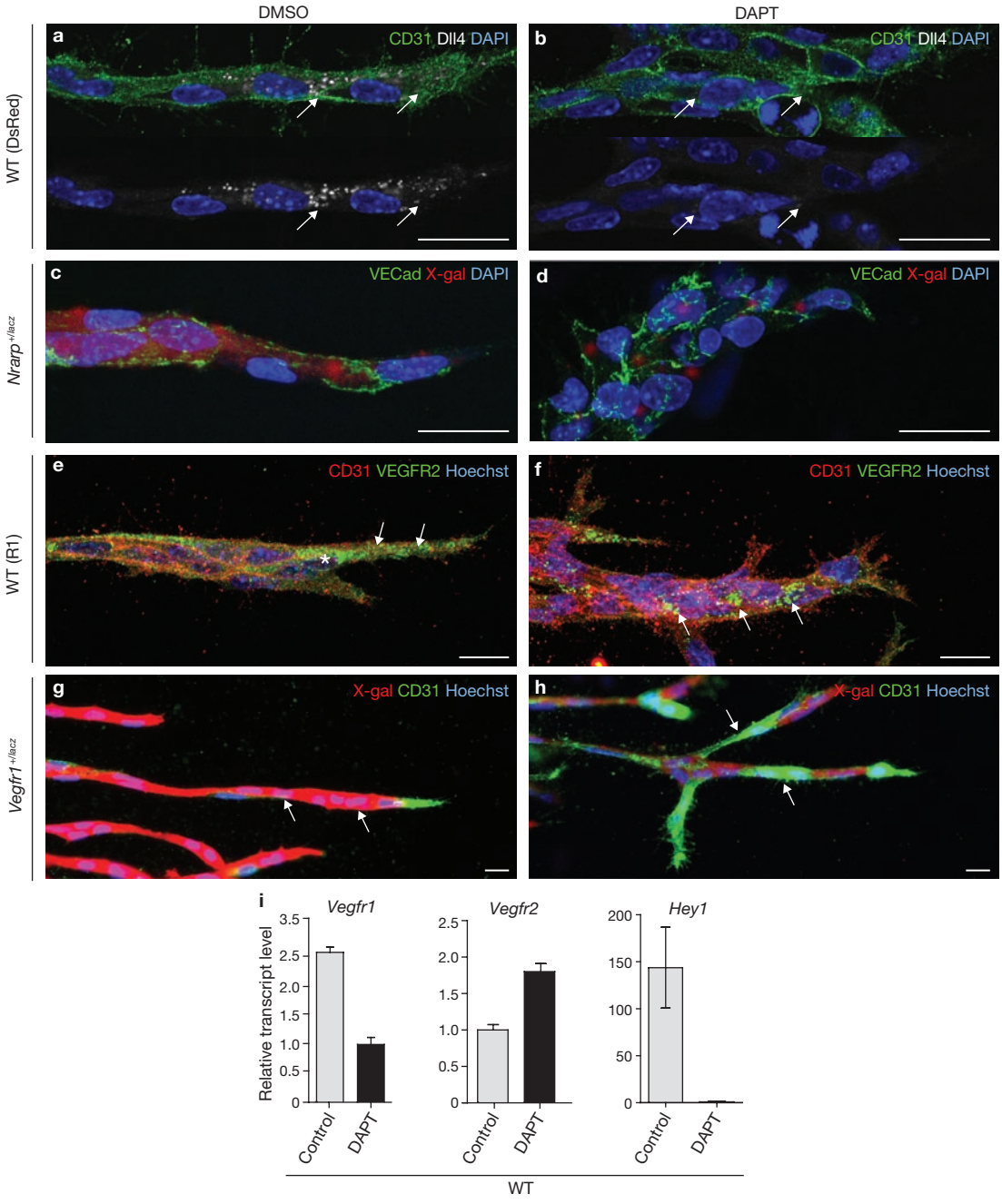

Figure 3 Notch regulates Dll4, VEGFR2 and VEGFR1 in sprouting embryoid bodies. (**a**–**h**) Representative fluorescence microscopy images of embryoid bodies before and after DAPT treatment. (**a**, **b**) Dll4 staining in wild-type embryoid bodies. Arrows indicate location of Dll4. (**c**, **d**) Location of Nrarp (red) in *Nrarp*$^{+/lacz}$ embryoid bodies was assessed by treatment with X-gal and staining for VE-Cadherin (green). Note decreased *Nrarp* expression with DAPT treatment **(d)**. **(e)** VEGFR2 (green, indicated by arrows) is most prominent in the tip cell (asterisk) but also present in subsets of stalk cells. (**f**) DAPT treatment increases and disrupts the spatial distribution of VEGFR2 (arrows). (**g**) Assessment of *Vegfr1* promoter activity by X-gal treatment (red) in endothelial sprouts from *Vegfr1*$^{+/lacZ}$ embryoid bodies. Endothelial cells were identified by CD31 immunostaining (green; masked by signal from X-gal reaction, as indicated by arrows). Some tips have very low or undetectable *Vegfr1* expression. (**h**) DAPT treatment decreases expression of VEGFR1 (arrows). (**i**) Real-time quantitative PCR of wild-type embryoid bodies cultured in collagen with VEGF alone or in combination with DAPT. Values indicate mean ± s.d.

Endothelial cells derived from embryonic stem cells heterozygous for the *Vegfr2* allele, generated through insertion of the enhanced green fluorescent protein (*egfp*) sequence into exon one of the *Vegfr2* gene (*Vegfr2*$^{+/egfp}$), had approximately half the VEGFR2 levels of wild-type cells (Supplementary Information, Fig. S2a). Embryoid bodies derived solely from *Vegfr2*$^{+/egfp}$ cells are indistinguishable from those derived from wild-type cells, showing similar density and radial expansion of vascular sprouts (Supplementary Information, Fig. S2b). When mixed with wild-type cells in a 1:1 ratio in mosaic cultures, *Vegfr2*$^{+/egfp}$ cells contribute to the developing vasculature to the same extent as wild-type cells (Supplementary Information, Fig. S2c). However, *Vegfr2*$^{+/egfp}$ cells contributed to only 13% of the tip cells (Fig. 1e, f, l), suggesting that the

reduced *Vegfr2* levels selectively impair the ability of cells to become tip cells when mixed with wild-type cells. This was independently verified with different *Vegfr2* heterozygous embryonic stem cell lines (*Vegfr2*$^{+/lacZ}$; tip contribution of 4.4% ± 0.37, mean ± s.e.m.). The reduced frequency of *Vegfr2* heterozygote cells occupying the tip position was surprisingly robust to alterations of the mixing ratio. With an increasing ratio of *Vegfr2*$^{+/egfp}$ cells to wild-type, the wild-type cells still contributed to approximately 80% of the tip cells in a 8:2 mixture, and to more than 60% in a 9:1 mixture (Supplementary Information, Fig. S3), whereas the stalks of the sprouts were almost exclusively derived from *Vegfr2*$^{+/egfp}$ cells. Two cell lines heterozygous for *Vegfr2* (*Vegfr2*$^{+/egfp}$ and *Vegfr2*$^{+/lacz}$) mixed with each other in 1:1 mosaic embryoid bodies were equally capable of contributing to the tip cell population (45.8% and 54.2%, respectively). This demonstrates that *Vegfr2* levels do not control the intrinsic ability of endothelial cells to become tip or stalk cells, but that differences in *Vegfr2* levels between two cells affect which of the cells will become a tip cell, in a competitive manner.

To investigate the role of differential *Vegfr1* levels in tip cell selection, we studied angiogenic sprouting in chimaeric cultures of wild-type (DsRed) and *Vegfr1*$^{+/lacz}$ embryonic stem cells at a 1:1 ratio. The developing vasculature was highly mosaic (Fig. 1g, h). Despite a slightly reduced overall contribution of *Vegfr1*$^{+/lacz}$ cells to endothelial cells (33%; Supplementary Information, Fig. S2c), 70% of the tip cells were derived from the *Vegfr1* heterozygote lineage (Fig. 1l). Thus, a cell with lower *Vegfr1* expression has a higher probability of acquiring the leading position, whereas a cell with lower *Vegfr2* expression has reduced ability to take the lead, when competing with a wild-type neighbouring cell.

Competition in chimaeric mouse retinal vasculature

To test whether the competition principles apply *in vivo*, we generated chimaeric mice and analysed the contribution of embryonic stem cells to the tip and stalk cell populations in developing retinal vasculature. Morulas or blastocysts of unmodified mice or wild-type mice with DsRed or eGFP expression were injected with wild-type cells (expressing DsRed), *Vegfr2*$^{+/egfp}$-, or *Vegfr1*$^{+/lacz}$-embryonic stem cells, alone or in combination. After 2 days they were transferred to pseudo-pregnant females. Retinas from chimaeric pups were fixed at postnatal day (P) 5.5 and processed for immunofluorescence microscopy and/or enzymatic analysis. The contribution of injected embryonic stem cells to the retinal vasculature ranged from 0 to 100%. In retinas with partial contribution to the vasculature most regions were highly mosaic. In wild-type hosts injected with wild-type embryonic stem cells expressing DsRed, both genotypes contributed to endothelial tip and stalk cells (Fig. 1i, see also Fig. 7a–f).

Endothelial cells derived from *Vegfr2*$^{+/egfp}$ embryonic stem cells injected into wild-type hosts were traced by their eGFP expression. In mosaic regions of the developing vascular front, *Vegfr2* heterozygote cells were under-represented in the tip cell population, despite comprising the majority of stalk cells in close vicinity (Fig. 1j, m). *Vegfr1*$^{+/lacz}$ embryonic stem cells were injected into blastocysts expressing DsRed or eGFP; *Vegfr1*$^{+/lacz}$ embryonic stem cells were then identified by treatment with X-gal (5-bromo-4-chloro-3-indolyl-β-D-galactoside) and the lack of DsRed or eGFP fluorescence. Similarly to *in vitro*, the overall contribution of *Vegfr1*$^{+/lacz}$ cells to the vasculature was generally lower, compared with wild-type- and *Vegfr2*$^{+/egfp}$-cells. Nevertheless, in retinas where cells

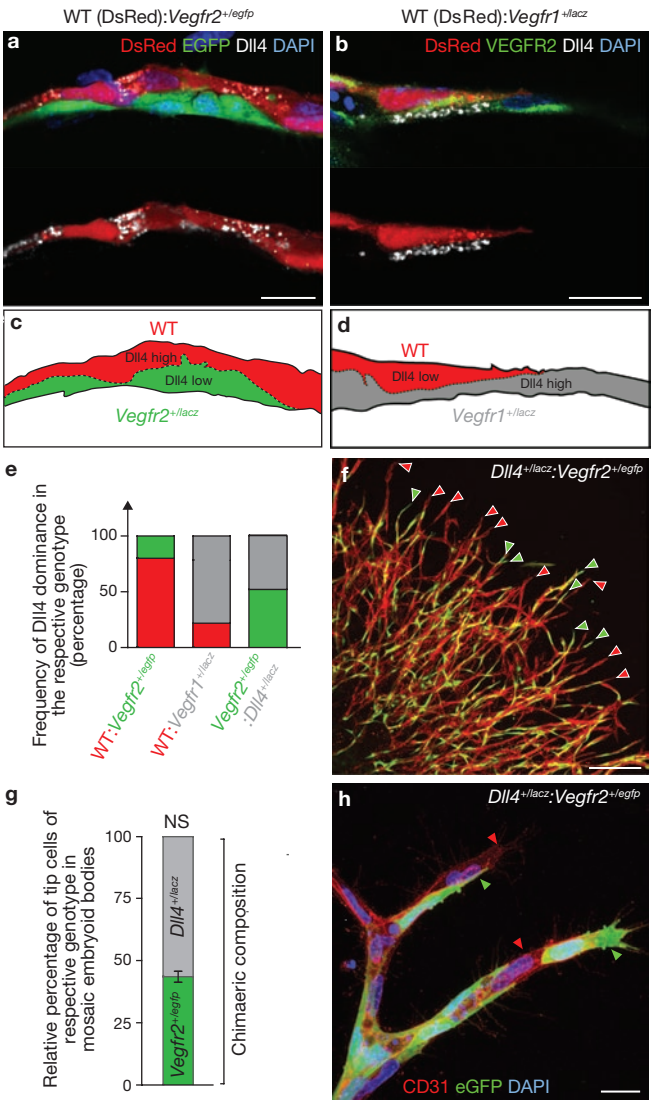

Figure 4 VEGFR-mediated Dll4 expression dictates tip/stalk phenotype in a cell–cell dependent manner. (**a**) Representative immunofluorescence microscopy images of the stalk region of a mosaic vascular sprout of wild-type cells (expressing DsRed; red) and *Vegfr2*$^{+/egfp}$ cells (green) showing high levels of Dll4 (white) in wild-type cells, compared with the adjacent *Vegfr2*$^{+/egfp}$ cells. (**b**) Representative immunofluorescence microscopy images of a mosaic vascular sprout of wild-type cells (expressing DsRed, red) and *Vegfr1*$^{+/lacz}$ cells showing high levels of Dll4 (white) in the *Vegfr1*$^{+/lacz}$ cells, compared with the adjacent wild-type (red) cells. Scale bars, **a**, **b**, 20 μm. (**c**) Schematic representation of cellular borders in **a**. (**d**) A schematic representation of cellular borders in **b**. (**e**) Pairwise comparison of Dll4 protein levels in the indicated chimaeric embryoid bodies. Dll4 levels are reduced in *Vegfr2* heterozygote endothelial cells, compared with adjacent wild-type endothelial cells in 82% of cellular pairs analyzed ($n = 77$). Dll4 levels are induced in *Vegfr1* heterozygote endothelial cells, compared with adjacent wild-type endothelial cells in 80% of cellular pairs analyzed ($n = 51$). Dll4 levels are higher in a similar percentage of *Vegfr2*$^{+/egfp}$ cells (52%; $n = 47$), compared with adjacent *Dll4*$^{+/lacz}$ cells. (**f**) Representative immunofluorescence microscopy image of a *Dll4*$^{+/lacz}$:*Vegfr2*$^{+/egfp}$ chimaera stained for CD31 (red) to assess contribution of *Dll4*$^{+/lacz}$ (red arrow heads) and *Vegfr2*$^{+/egfp}$ (green arrow heads) cells to the tip-cell position. (**g**) Quantification of tip cells with the indicated genotype in *Vegfr2*$^{+/egfp}$:Dll4$^{+/LacZ}$ embryoid bodies. Number of counted tips: 390. Values represent mean ± s.e.m. ($n = 4$). NS, not statistically different from wild-type:wild-type chimaeras in Figure 1l. (**h**) Representative image of the mosaic sprouts at higher magnification. Red arrowheads indicate *Dll4*$^{+/lacz}$ endothelial cells, whereas green arrowheads indicate *Vegfr2*$^{+/egfp}$ endothelial cells.

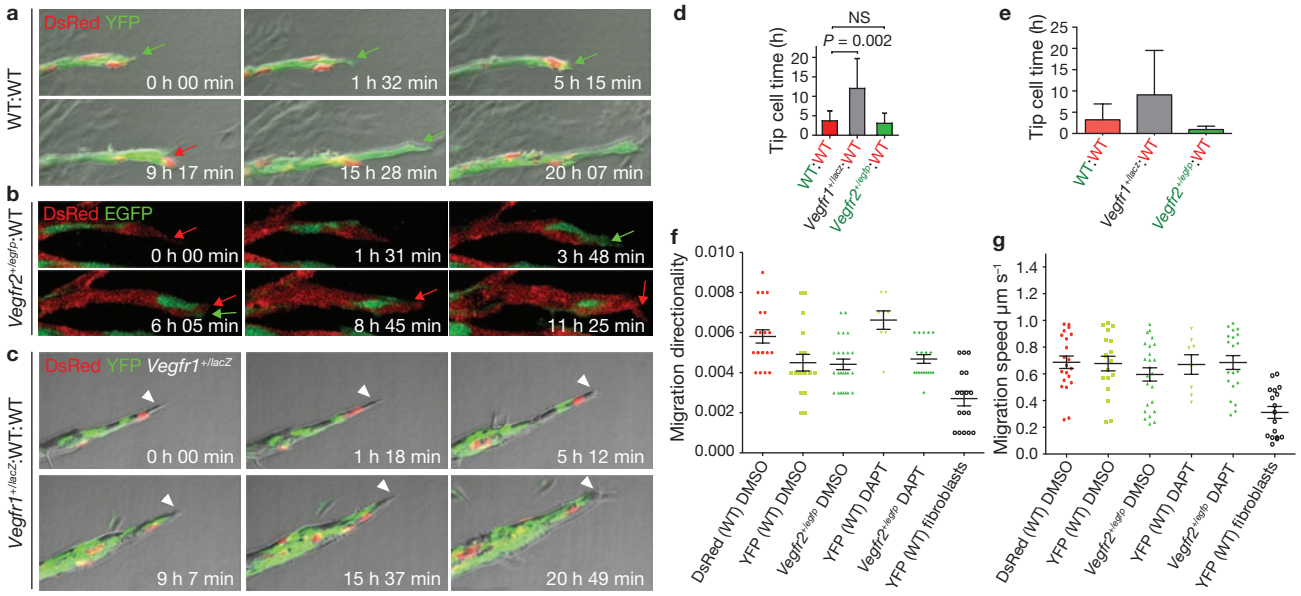

Figure 5 Dynamic observations of tip cell shuffling in sprouting angiogenesis. (**a**) Time-lapse microscopy images of chimaeric embryoid bodies of wild-type cells expressing DsRed (red) and wild-type cells expressing YFP (green). Red arrow indicates when a green cell is overtaken by a red. (**b**) Time-lapse microscopy images of chimaeric embryoid bodies of cells expressing *Vegfr2*$^{+/egfp}$ (green) and wild-type cells expressing DsRed (red). The green cell at the tip is overtaken by a wild-type cell after approximately 2 h and 17 min. (**c**) Triple chimaeric embryoid bodies composed of *Vegfr1*$^{+/lacz}$ cells (non-fluorescent cells, arrowhead), wild-type cells expressing DsRed (red) and wild-type cells expressing YFP (green). The *Vegfr1*$^{+/lacz}$ cell remains in tip position. (**d**) Quantification by time-lapse microscopy of how long a cell that reaches the tip stays there until it is overtaken. *Vegfr1*$^{+/lacz}$ stay on average 12 h at the tip, *Vegfr2*$^{+/egfp}$ cells stay on average 3.1 h in the tip position when competing with wild-type cells. Wild-type cells stay on average 3.7 h at the tip when mixed with other traceable wild-type cells. Values represent mean ± s.e.m of time at tip of wild-type in wild-type:wild-type chimaeras (n = 19); *Vegfr1*$^{+/lacz}$:wild-type:wild-type chimaeras (n = 10); *Vegfr2*$^{+/egfp}$:wild-type chimaeras (n = 12). **(e)** Computer-simulated tip-cell repositioning in chimaeras. Tip cell duration of the various genotypes match the biological data when simulated based on the VEGF–VEGFR–Dll4–Notch1–VEGFR signalling circuit (for details see Supplementary Information, material). (**f, g**) Quantification of migration directionality (**f**) and average migration speed (**g**) of wild-type (DsRed and YFP) and *Vegfr2*$^{+/egfp}$ endothelial cells or wild-type (YFP) fibroblasts in different chimaeric embryoid bodies, with and without DAPT treatment. For details on segmentation, see Methods.

heterozygous for *Vegfr1* did contribute, few were observed in the central region of the retinal vasculature and the majority were close to the sprouting front, often contributing to the tip cell position (Fig. 1k and Supplementary Information, Fig. S4a). Occasionally, we also observed LacZ-negative tip cells derived from *Vegfr1*$^{+/lacz}$ embryonic stem cells, which was probably a consequence of the reduced *Vegfr1* promoter activity at the tip position (Supplementary Information, Fig. S4a). Quantification of the relative contribution to the vascular front (tip region) and more central retina (stalk region; see Supplementary Information, Fig. S4b, c for method details) confirmed enrichment of *Vegfr1* heterozygote cells at the front (Fig. 1m).

Low Dll4 levels and increased Notch signalling cell-autonomously reduce tip cell potential in competition

To understand the role of Dll4–Notch signalling in the competition process, we investigated sprouting angiogenesis and cellular distribution with genetic and pharmacological inhibition of Notch signalling activity. Inhibition of γ-secretase by DAPT (N-[N-(3,5-difluorophenacetyl)-L-alanyl]-S-phenylglycine t-butylester) abolishes Notch signalling, leading to a strong hyper-sprouting phenotype *in vitro* and *in vivo*[15,28,29]. Treatment of wild-type (R1) embryoid bodies with DAPT led to a similar hypersprouting phenotype (Fig. 2a, b). Embryoid bodies derived from *Dll4*$^{+/lacz}$ and *Dll4*$^{lacz/lacz}$ embryonic stem cells showed marked *lacz* expression in the sprouts (Supplementary Information, Fig. S5), and a gene-dosage dependent hypersprouting phenotype similar to what has been reported *in vivo*. DAPT treatment of wild-type cells or cells heterozygous for *Dll4* produced a hypersprouting phenotype very similar to *Dll4*-null embryonic stem cells, whereas DAPT treatment of *Dll4*-null cells did not lead to a further increase in sprouting, indicating that the DAPT phenotype is primarily related to the inhibition of Dll4–Notch signalling (Fig. 2c–f). In chimaeric embryoid bodies, *Dll4* heterozygote cells had reduced Dll4 protein levels, and the majority of the tip cells were wild type (Fig. 2g, i, k). Inhibition of Notch activity by DAPT treatment restored the balance of Dll4 heterozygous and wild-type cells at the leading position (Fig. 2h, k), confirming that Dll4 levels affect the competition for the tip cell through the activation of Notch.

Nrarp heterozygote cells competing with wild-type cells contributed to only 30% of the tip population (Fig. 2j, k), demonstrating that higher Notch activity, caused by diminished negative Notch intracellular domain regulation[30,31], reduces the potential of endothelial cells to adopt the tip cell position.

Notch signalling regulates expression and spatial distribution of Dll4, VEGFR2 and VEGFR1

To investigate the relationship between Notch signalling and expression of Dll4, VEGFR2 and VEGFR1, we analysed the spatial distribution of these molecules in the presence or absence of Notch signalling. Specific Dll4 protein labelling was localized to cytoplasmic vesicles in

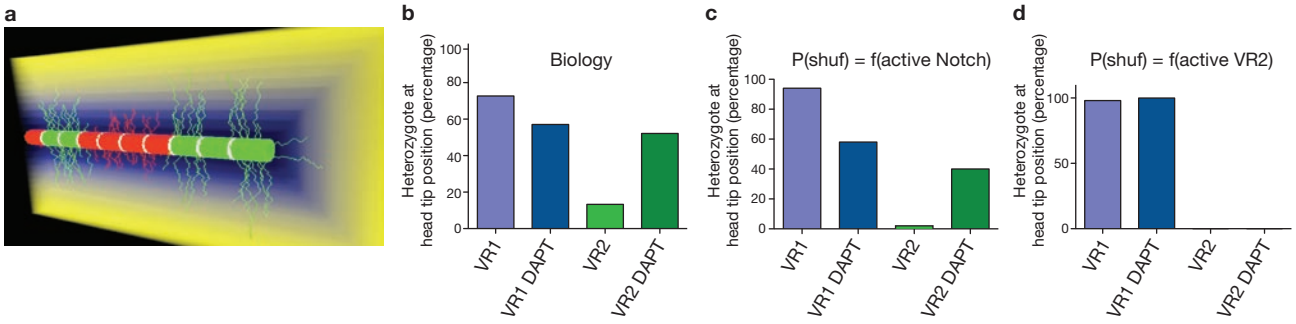

Figure 6 Computational modelling suggests regulation of cell shuffling by Notch. (**a**) Representative image from *Vegfr1*$^{+/-}$ (VR1):wild-type chimaeric-sprout simulation (wild-type cells; red, VR1 heterozygote cells; green). VEGF gradient is shown (low to high; blue to yellow). Leading tip cell is on the right of the image. Other uninhibited tip cells are generated in the stalk of the sprout by Dll4–Notch lateral inhibition, which then shuffle up and compete for the head tip position. (**b**–**d**) Simulation of cell type at the tip of sprouts as a function of Notch activity (**c**) or VEGFR2 (VR1) activity (**d**), compared with biological data (**b**). The simulated sprout consisted of heterozygote cells and wild-type cells (1:1) randomly arranged, and the biological data were from chimaeric 1:1 experiments. When using the active VR2 shuffling function, the DAPT simulation no longer matched the biological results (**d**).

a salt-and-pepper distribution in sprouts of wild-type endothelial cells (Fig. 3a and Supplementary Information, Fig. S6). Many leading tip cells exhibited abundant staining, whereas neighbouring stalk cells frequently showed little or no Dll4 signal. DAPT treatment consistently reduced the vesicular Dll4 protein localization, indicating that full endothelial *Dll4* expression requires Notch signalling activity (Fig. 3b).

Mosaic β-galactosidase expression in *Nrarp*$^{+/lacz}$ cells, signifying Notch signalling, was reduced by DAPT treatment (Fig. 3c, d and Supplementary Information, Fig. S7a–d). VEGFR2-antibody labelling revealed the strongest staining in most of the leading tip cells. Labelling was observed both on the membrane and in cytoplasmic vesicles (Fig. 3e) consistent with previous findings of abundant endosomal VEGFR2 localization in VEGFA-stimulated endothelial cells[32]. Inhibition of Notch signalling by DAPT treatment upregulated VEGFR2 and enhanced the vesicular localization (Fig. 3f). *Vegfr1*$^{+/lacz}$ cells frequently had lower LacZ levels in the tip cells, and higher levels in stalk cells, which was reduced by DAPT treatment (Fig. 3g, h). Quantitative real-time PCR (QPCR) analysis of wild-type embryonic stem cells confirmed the Notch-dependent down-regulation of *Vegfr2* and upregulation of *Vegfr1* (Fig. 3i).

VEGFR level-mediated competition is strictly Notch dependent

The observed importance of VEGFR levels and Dll4–Notch activation in the competition process is consistent with the hypothesis that VEGFR levels function as Notch effectors during tip/stalk cell selection. Operation of such a mechanism predicts that genetically mosaic vascular sprouts would select for tip cells with highest VEGFR2 and/or lowest VEGFR1 even in the absence of Notch signalling. To test this hypothesis, we treated *Vegfr2*$^{+/egfp}$:wild-type (DsRed) chimaeric embryoid bodies with DAPT. Unexpectedly, DAPT treatment completely abrogated the advantage of cells with higher *Vegfr2* levels in the tip-cell selection process (Fig. 2k). DAPT treatment of *Vegfr1*$^{+/lacz}$:wild-type (DsRed) cultures also abolished the genotypic over-representation of *Vegfr1* heterozygote cells in the tip cell position (Fig. 2k).

One possible explanation could be that the loss of Notch-dependent regulation of *Vegfr2* on DAPT treatment overrides the gene-dosage effect, so that heterozygote cells and wild-type cells no longer show differences in *Vegfr2* expression. However QPCR analysis of endothelial cells from chimaeric embryoid bodies sorted by FACS (fluorescence-activated cell sorting) demonstrated that *Vegfr2* heterozygote cells express half the amount of *Vegfr2* mRNA when compared with wild-type DsRed-expressing cells (Fig. 2l), confirming that the *Vegfr* gene dosage is reflected in mRNA expression. DAPT treatment of the chimaeric embryoid bodies increased the expression of *Vegfr2* in both cell types (Fig. 2l). However, wild-type cells still expressed double the amount of *Vegfr2* compared to *Vegfr2* heterozygote cells, confirming that cells with twice as much *Vegfr2* expression no longer have a competitive advantage when Notch signalling is inhibited. Thus, Notch signalling is essential for cells to become selected according to their VEGFR levels, indicating for the first time that VEGFR levels mainly operate upstream of Dll4–Notch in the selection process.

VEGFR2 and Dll4 levels correlate in endothelial cells of sprouting vessels

A direct comparison of Dll4 immunolabelling in pairs of adjacent *Vegfr2*$^{+/egfp}$ and wild-type (DsRed) endothelial cells in chimaeric embryoid bodies revealed higher expression of Dll4 in wild-type cells (Fig. 4a, c, e). The same wild-type (DsRed) cells showed consistently lower Dll4 levels than the *Vegfr1*$^{+/lacz}$ cells in mosaic cultures, suggesting that VEGFR2 levels or signalling correlate with Dll4 expression (Fig. 4b, d, e). FACS of *Vegfr2*$^{+/egfp}$ and DsRed endothelial cells from the chimaeric embryoid bodies followed by QPCR analysis confirmed that *Vegfr2* and *Dll4* levels also correlate at the mRNA level (Fig. 2l). In non-chimaeric embryoid bodies of *Vegfr2*$^{+/egfp}$ and DsRed cells, however, the total *Dll4* levels were indistinguishable (not shown). Thus, the amount of Dll4 produced is not a cell-intrinsic quality, but strictly depends on neighbourhood relationships when cells with different receptor levels compete.

To directly test whether the *Vegfr2* and *Dll4* levels are functionally linked during competition, we mixed *Vegfr2*$^{+/egfp}$ cells with *Dll4*$^{+/lacz}$ cells. Quantification of tip cell contribution in chimaeric embryoid bodies revealed no difference between the two populations (Fig. 4f–h), demonstrating that the disadvantage of a cell with reduced VEGFR2 levels can be counterbalanced by a reduced *Dll4* gene dosage in the competing cell.

Dynamic cell shuffling in angiogenic sprouts

The identification of cell competition for the tip position raises the question as to whether this is constant or recurring and how cell dynamics influence the process. To study dynamic cell behaviour, we established time-lapse confocal microscopy of the mosaic embryoid body cultures

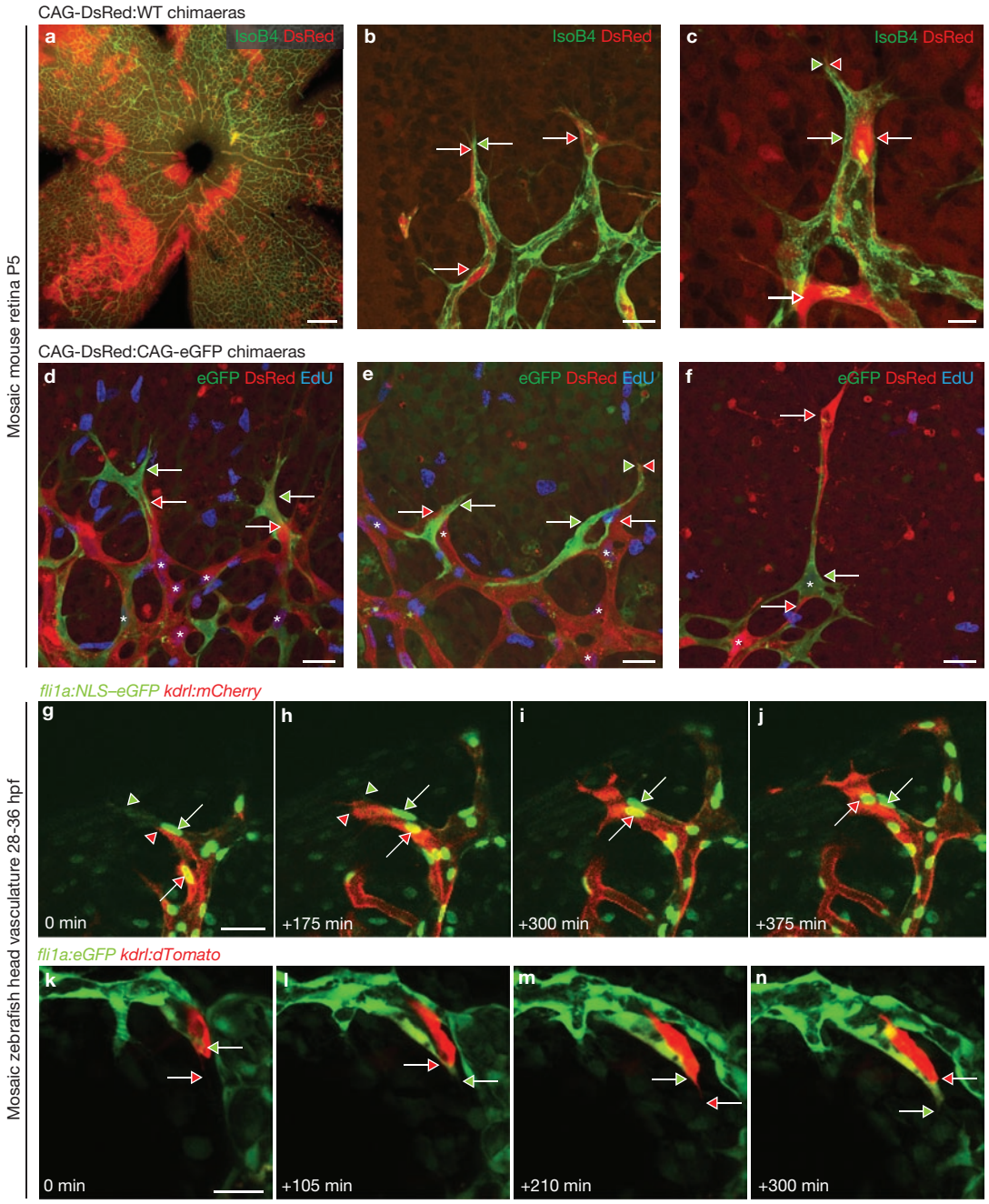

Figure 7 Dynamic position shuffling *in vivo*. (**a**–**c**) Fluorescence microscopy images of a whole mount-stained mosaic retina of a P5.5 pup derived from a wild-type blastocyst injected with wild-type embryonic stem cells expressing DsRed. Isolectin B4 (green) indicates sprouting vasculature. (**a**) An overview of the retina shows clonal expansion of DsRed-derived cells within the neuronal lineage. However the vessels are mosaic, with both genotypes represented as tip and stalk cells adjacent to one another (red and green arrows, **b** and **c**). (**d**–**f**) Fluorescence microscopy images of a retina derived from a blastocyst expressing eGFP injected with embryonic stem cells expressing DsRed. Endothelial stalk cells just behind the tips proliferate (asterisks) but the vascular region remains mosaic (green and red arrows), indicative of continuous cell shuffling. EdU staining (blue) indicates proliferating cells. (**g**–**j**) Representative images from confocal time-lapse microscopy of double transgenic zebrafish embryos (*kdrl:mCherry*, *fli1a:NLS–eGFP*). Filopodial dynamics and positioning of the cell body were monitored by location of mCherry andNLS–eGFP, respectively. Green arrow indicates the cell initially taking the tip cell position (with green arrowhead marking its filopodia); red arrow and arrowhead indicate cell taking over the tip cell position at later stages. See Supplementary Information, Movies S7and S8). (**k**–**n**) Representative images from confocal time-lapse microscopy of dTomato-labelled endothelial cells in a *fli1a:eGFP* transgenic zebrafish embryo. Red arrow indicates leading filopodia of the endothelial cell and green arrow indicates position of the tip cell. Endothelial cells gain and regain the distal tip as they shuffle along each other. See Supplementary Information, Movie S9. Scale bars: **a**, 250 μm; **b**, 25 μm; **c**, 10 μm; **d**–**f**, 25 μm; **g**, 25 μm; **k**, 25 μm.

over 1- to 4-day periods (Supplementary Information, Movie S1). Both wild-type and *Vegfr2*$^{+/egfp}$ cells migrated markedly within the sprouts, but *Vegfr2*$^{+/egfp}$ cells rarely reached the tip position and were rapidly overtaken by wild-type cells at this position. DAPT treatment restored the ability of *Vegfr2*$^{+/egfp}$ cells to gain and regain the tip position (Supplementary Information, Movie S2).

Image segmentation and cell tracking (Supplementary Information, Movie S3) showed that wild-type tip cells are overtaken by other wild-type cells on average after approximately 3.7 h (Fig. 5a, d and Supplementary Information, Movie S4). *Vegfr2*$^{+/egfp}$ cells persisted on average only 3.1 h at the tip position (not significantly different from wild-type; Fig. 5b, d, Supplementary Information, Movie S5). In contrast, *Vegfr1*$^{+/lacz}$ cells stayed in tip position for 12 h on average and showed a larger degree of variation (Fig. 5c, d, and Supplementary Information, Movie S6). Computational modelling confirmed the influence of VEGFR levels on tip cell duration (Fig. 5e).

Cell tracking demonstrated that wild-type cells (expressing DsRed or yellow fluorescent protein; YFP) and *Vegfr2*$^{+egfp}$ cells migrated at roughly similar velocity and with similarly persistent directionality (Fig. 5f, g). *Vegfr2* heterozygote cells showed a slightly greater spread in velocity and directionality, possibly because of the stronger Notch signalling they receive. However, DAPT treatment did not affect this pattern. Thus, cell migration speed does not constitute a major parameter in the competition for the tip.

Computational modelling suggests cell shuffling is regulated by Notch activity

To explore the regulation of cell shuffling and the effects of shuffling on the selection process, we modified the computational selection model into a directional sprout with a leading tip cell (Fig. 6a and Supplementary Information, methods). Cells were allowed to swap places with a neighbour towards the tip with a certain probability, modelled either as a function of VEGFR2 activity, or of Notch activity (see Supplementary Information, material). Both probability functions lead to a strong prevalence of wild-type cells over *Vegfr2* heterozygote cells, and of *Vegfr1* heterozygote cells over wild-type cells at the leading tip position, similar to the biological experiments. However, only the active Notch probability function reproduced the effect of DAPT, which fully abrogates the advantage of wild-type cells over *Vegfr2* heterozygote cells in tip cell competition (Fig. 6c), suggesting that dynamic position shuffling of endothelial cells is negatively regulated by Notch activity.

Dynamic competition and position shuffling *in vivo*

To understand whether dynamic competition and position shuffling is relevant for sprouting vessels *in vivo*, we studied mosaic vessels in chimaeric mouse retinas and in zebrafish (*Danio rerio*) embryos (Fig. 7). In mouse chimaeras, clonal expansion of the embryonic stem-cell-derived DsRed-positive populations was prominent in the neural retina (Fig. 7a). However, DsRed-positive endothelial cells rarely clustered together, which gave a highly mosaic vasculature. Single DsRed cells forming part of the tip structure were frequently separated from the next DsRed positive cell by unlabelled cells (Fig. 7c). The lack of clonal expansion in the stalk region indicates that cells disperse after cell division. Direct observations of retinas from chimaeric CAG-DsRed and CAG-eGFP mice combined with EdU (5-ethynyl-2'-deoxyuridine) pulse-labelling of proliferating cells confirmed that endothelial cells proliferate, but daughter cells seem to exchange positions with other endothelial cells (Fig. 7d–f).

To directly study dynamic endothelial cell behaviour *in vivo*, we performed time-lapse confocal microscopy of zebrafish embryos (Fig. 7g–n). In one approach, we crossed zebrafish lines expressing endothelial nuclear GFP (*fli1a:NLS–GFP*) and cytosolic mCherry (*kdrl:mCherry*). Imaging vessel development in the head region, we observed stalk cells overtaking tip cells, and former tip cells migrating back to the base of the sprout (Fig. 7g–j and Supplementary Information, Movies S7 and S8). In a second approach, we generated sparse clones of dTomato-labelled endothelial cells by injecting a *pTol2-kdrl:dTomato* plasmid together with transposase into *fli1a:eGFP* embryos. Time-lapse confocal microscopy demonstrated how endothelial cells compete dynamically for the tip position (Fig. 7k–n and Supplementary Information, Movie S9).

DISCUSSION

Here, we show the importance of cellular competition during angiogenic sprouting. Mosaic analysis *in silico, in vitro* and *in vivo* demonstrate that reduced *Vegfr2* levels provide a cell-autonomous disadvantage for cells to adopt the tip cell position, whereas reduced *Vegfr1* levels provide a cell-autonomous advantage for the tip cell position. Tip cell competition through *Vegfr* levels establishes a biological function for the dynamic *Vegfr* regulation during sprouting angiogenesis. *Vegfr* levels function upstream of Notch signalling in competitive tip cell selection, by controlling *Dll4* expression. The amount of *Dll4* expressed in a single endothelial cell is strictly dependent on its environment and is controlled by the relative *Vegfr* levels between the cell and its neighbours.

Our results with chimaeras, and computer simulation, indicate that a Notch-dependent regulation of *Vegfr2* could function to limit tip cell formation from the stalk. However, the DAPT-treatment experiments demonstrate that cells with lower *Vegfr2* levels are not inhibited from becoming tip cells, and that they can migrate, proliferate and sprout in the same way as wild-type cells. Endothelial cells with 50% reduction in *Vegfr2* levels, compared with wild-type, contribute equally to the developing vasculature in chimaeras, which suggests that endothelial cells with higher *Vegfr2* have no advantage over heterozygote cells in the initial phases of vasculogenic progenitor induction and subsequent proliferation. *Vegfr2* levels also do not seem to affect endothelial cell survival under normal developmental conditions. *Vegfr2* heterozygote cells only show a disadvantage in tip cell selection. Thus, endothelial cell induction, proliferation and survival are not affected by a 50% reduction in *Vegfr2* and do not seem to involve cell–cell competition mechanisms, whereas tip-cell selection is strictly competitive and dependent on the level of *Vegfr2*.

Recent studies indicated that VEGFR1 affects endothelial cell proliferation, vessel morphogenesis and even tip cell guidance in a non-cell autonomous function primarily through its soluble isoform[11,33]. Membrane bound and soluble VEGFR1 might pattern the microenvironment by sequestering VEGF-A. Regions of low VEGFR1 will theoretically contain higher free concentrations of VEGF-A, and endothelial cells in this region will have more VEGF-A available for activation of VEGFR2. Our results do not distinguish between soluble or transmembrane forms of VEGFR1, but demonstrate that *Vegfr1* is prominently regulated by Notch signalling, and that *Vegfr1* levels strongly affect tip cell competition, causing cells with lower *Vegfr1* expression to dominate the tip cell position. *Vegfr1* heterozygote cells produce higher levels of Dll4 mRNA and protein when competing with wild-type cells, which affects both the frequency of tip-cell selection and the duration of tip cell positioning.

Vegfr3 is also expressed in endothelial tip cells, and negatively regulated by Notch[34], raising the possibility that VEGFR3 might also influence tip cell selection. Indeed, we have observed that cells with lower *Vegfr3* levels dominate the tip position in competition with wild-type cells (unpublished data). VEGFR3, stimulated by VEGF-C, seems to promote the conversion of tip into stalk cells through reinforcing Notch signalling (K. Alitalo, personal communication). Thus, all three VEGF receptor tyrosine kinases are regulated by Notch signalling, and differential expression levels of these proteins influence the competition for the tip position. However, whereas *Vegfr1* and *Vegfr2* affect Dll4 production, *Vegfr3* seems to feedback onto Notch levels.

Dynamic imaging identified an unexpected degree of cell rearrangements along the length of the lumenized sprouts, both in the embryoid bodies, and *in vivo*. The absence or presence of flow in the proximal vascular plexus has little effect on cell shuffling, confirming that cellular processes regulating angiogenic sprouting are largely independent of flow[35]. Conceptually, position shuffling will constantly change neighbourhood relationships and therefore should trigger recurrent Dll4–Notch-mediated competition. Cells with higher *Vegfr2* and lower *Vegfr1* expression will overtake their neighbours in this process. A similar cell rearrangement has been reported in *Drosophila* trachea development, where cells with higher Fgfr levels switch positions with their local neighbours[3]. Mosaic analysis of mouse ureteric bud formation and mammary gland morphogenesis also showed that cells with higher growth factor receptor levels will cluster closest to the ligand source[36,37]. Such a mechanism seems particularly relevant for the generation of local budding domains where a group of epithelial cells will collectively respond by forming a multicellular budding tip.

However, in angiogenic sprouting, and in *Drosophila* trachea, branching morphogenesis relies on one or two tip cells dynamically selected to lead the new branch. Cell shuffling in such a system could be counterproductive as the established salt and pepper pattern of tip and stalk cells, important for branching, would be constantly disrupted, potentially leading to clustering of cells with similar receptor levels at the tip. Our computational analysis indicates that such a clustering effect may indeed occur (Supplementary Information, Movies S10 and S11), but is transient, and even cyclic, as Notch signalling effectively re-establishes a mixed pattern of cells with high and low receptor levels.

From a systems perspective, it is desirable to understand whether there is a functional advantage in exchanging the leading cell during vascular sprouting. The mechanism of competition seems to be the cause for position exchange. Given that the competition utilizes the levels of receptors for the factor guiding directional migration (VEGF-A), it is tempting to speculate that competition and position exchange serve to couple VEGFR levels to leadership to ensure that at any time, the leading cell of a vascular sprout is ideally equipped to sense the direction of the VEGF-A gradient. A tip cell erroneously migrating towards less VEGF-A will not be able to produce as much Dll4, allowing the challenging neighbour to gain a competitive advantage, particularly if the latter branches off in a new direction. Directionality of the guided sprouting process is thus perhaps not achieved at the cellular level of a single tip cell, but is rather the result of a population behaviour, in which the migration direction of a single cell is not always optimal, and the reiterative shuffling coupled to VEGFR–Dll4–Notch feedback ensures migration continues towards the highest concentration of VEGF-A. □

METHODS

Methods and any associated references are available in the online version of the paper at http://www.nature.com/naturecellbiology/

Note: Supplementary Information is available on the Nature Cell Biology website

ACKNOWLEDGEMENTS

We would like to thank the Cancer Research UK (CRUK) Light Microscopy facility, P. Jordan, the Protein Purification lab, S. Kjaer , J. Yang and J. Ure. We thank D. Barr and I. Moal for simulation and analysis work performed in the Biomolecular Modelling Laboratory CRUK, D. Sauvaget and J. Babbage for technical assistance and B. Thompson for comments on the manuscript. The authors are supported by CRUK, the Lister Institute of Preventive Medicine, the European Molecular Biology Organization (EMBO) Young Investigator Programme, the Fondation Leducq Transatlantic Network of Excellence ARTEMIS (H.G.), the Leukaemia Research Fund (to A.M.) and an EMBO long-term post-doctoral fellowship (to L.J.). We thank J. van Rheenen for discussions and assistance on the SP5 microscope (Leica Microsystems; equipment grant from the Dutch Organization of Scientific Research; NOW, 175.010.2007.007). We also thank A. de Graaff (M.Sc.) and the Hubrecht Imaging Centre (HIC) for imaging support. B.P. and S.S.-M. were supported by the Nederlandse Akademie van Wetenschappen (KNAW).

COMPETING FINANCIAL INTERESTS

The authors declare no competing financial interests.

Published online at http://www.nature.com/naturecellbiology
Reprints and permissions information is available online at http://npg.nature.com/reprintsandpermissions/

1. Johnston, L. A. Competitive interactions between cells: death, growth, and geography. *Science* **324,** 1679–1682 (2009).
2. Gerhardt, H. *et al.* VEGF guides angiogenic sprouting utilizing endothelial tip cell filopodia. *J. Cell Biol.* **161,** 1163–1177 (2003).
3. Ghabrial, A. S. & Krasnow, M. A. Social interactions among epithelial cells during tracheal branching morphogenesis. *Nature* **441,** 746–749 (2006).
4. Affolter, M. & Caussinus, E. Tracheal branching morphogenesis in *Drosophila*: new insights into cell behaviour and organ architecture. *Development* **135,** 2055–2064 (2008).
5. Roca, C. & Adams, R. H. Regulation of vascular morphogenesis by Notch signaling. *Genes Dev.* **21,** 2511–2524 (2007).
6. Ruhrberg, C. *et al.* Spatially restricted patterning cues provided by heparin-binding VEGF-A control blood vessel branching morphogenesis. *Genes Dev.* **16,** 2684–2698 (2002).
7. Olsson, A. K., Dimberg, A., Kreuger, J. & Claesson-Welsh, L. VEGF receptor signalling - in control of vascular function. *Nat. Rev. Mol. Cell Biol.* **7,** 359–371 (2006).
8. Hiratsuka, S., Minowa, O., Kuno, J., Noda, T. & Shibuya, M. Flt-1 lacking the tyrosine kinase domain is sufficient for normal development and angiogenesis in mice. *Proc. Natl Acad. Sci. USA* **95,** 9349–9354 (1998).
9. Park, J. E., Chen, H. H., Winer, J., Houck, K. A. & Ferrara, N. Placenta growth factor. Potentiation of vascular endothelial growth factor bioactivity, *in vitro* and *in vivo*, and high affinity binding to Flt-1 but not to Flk-1/KDR. *J. Biol. Chem.* **269,** 25646–25654 (1994).
10. Fong, G. H., Rossant, J., Gertsenstein, M. & Breitman, M. L. Role of the Flt-1 receptor tyrosine kinase in regulating the assembly of vascular endothelium. *Nature* **376,** 66–70 (1995).
11. Kappas, N. C. *et al.* The VEGF receptor Flt-1 spatially modulates Flk-1 signaling and blood vessel branching. *J. Cell Biol.* **181,** 847–858 (2008).
12. Carmeliet, P. *et al.* Abnormal blood vessel development and lethality in embryos lacking a single VEGF allele. *Nature* **380,** 435–439 (1996).
13. Ferrara, N. *et al.* Heterozygous embryonic lethality induced by targeted inactivation of the VEGF gene. *Nature* **380,** 439–442 (1996).
14. Hellstrom, M. *et al.* Dll4 signalling through Notch1 regulates formation of tip cells during angiogenesis. *Nature* **445,** 776–780 (2007).
15. Leslie, J. D. *et al.* Endothelial signalling by the Notch ligand Delta-like 4 restricts angiogenesis. *Development* **134,** 839–844 (2007).
16. Lobov, I. B. *et al.* Delta-like ligand 4 (Dll4) is induced by VEGF as a negative regulator of angiogenic sprouting. *Proc. Natl Acad. Sci. USA* **104,** 3219–3224 (2007).
17. Siekmann, A. F. & Lawson, N. D. Notch signalling limits angiogenic cell behaviour in developing zebrafish arteries. *Nature* **445,** 781–784 (2007).
18. Suchting, S. *et al.* The Notch ligand Delta-like 4 negatively regulates endothelial tip cell formation and vessel branching. *Proc. Natl Acad. Sci. USA* **104,** 3225–3230 (2007).
19. Williams, C. K., Li, J. L., Murga, M., Harris, A. L. & Tosato, G. Up-regulation of the Notch ligand Delta-like 4 inhibits VEGF-induced endothelial cell function. *Blood* **107,** 931–939 (2006).
20. Harrington, L. S. *et al.* Regulation of multiple angiogenic pathways by Dll4 and Notch in human umbilical vein endothelial cells. *Microvasc. Res.* **75,** 144–154 (2008).

21. Holderfield, M. T. *et al.* HESR1/CHF2 suppresses VEGFR2 transcription independent of binding to E-boxes. *Biochem. Biophys. Res. Commun.* **346,** 637–648 (2006).
22. Suchting, S. *et al.* Negative regulators of vessel patterning. *Novartis Found Symp.* **283,** 77–80; discussion 80–86, 238–241 (2007).
23. Hayashi, H. & Kume, T. Foxc transcription factors directly regulate Dll4 and Hey2 expression by interacting with the VEGF-Notch signaling pathways in endothelial cells. *PLoS ONE* **3**, e2401 (2008).
24. Liu, Z. J. *et al.* Regulation of Notch1 and Dll4 by vascular endothelial growth factor in arterial endothelial cells: implications for modulating arteriogenesis and angiogenesis. *Mol. Cell Biol.* **23,** 14–25 (2003).
25. Bentley, K., Gerhardt, H. & Bates, P. A. Agent-based simulation of notch-mediated tip cell selection in angiogenic sprout initialisation. *J. Theor. Biol.* **250,** 25–36 (2008).
26. Jakobsson, L., Domogatskaya, A., Tryggvason, K., Edgar, D. & Claesson-Welsh, L. Laminin deposition is dispensable for vasculogenesis but regulates blood vessel diameter independent of flow. *Faseb J.* **22,** 1530–1539 (2008).
27. Jakobsson, L., Kreuger, J. & Claesson-Welsh, L. Building blood vessels—stem cell models in vascular biology. *J. Cell Biol.* **177,** 751–755 (2007).
28. Sainson, R. C. *et al.* Cell-autonomous notch signaling regulates endothelial cell branching and proliferation during vascular tubulogenesis. *Faseb J.* **19,** 1027–1029 (2005).
29. Hellstrom, M. *et al.* Dll4 signalling through Notch1 regulates formation of tip cells during angiogenesis. *Nature* **445,** 776–780(2007).
30. Phng, L. K. *et al.* Nrarp coordinates endothelial Notch and Wnt signaling to control vessel density in angiogenesis. *Dev. Cell* **16,** 70–82 (2009).
31. Lamar, E. *et al.* Nrarp is a novel intracellular component of the Notch signaling pathway. *Genes Dev.* **15,** 1885–1899 (2001).
32. Gampel, A. *et al.* VEGF regulates the mobilization of VEGFR2/KDR from an intracellular endothelial storage compartment. *Blood* **108,** 2624–2631 (2006).
33. Chappell, J. C., Taylor, S. M., Ferrara, N. & Bautch, V. L. Local guidance of emerging vessel sprouts requires soluble Flt-1. *Dev. Cell* **17,** 377–386 (2009).
34. Tammela, T. *et al.* Blocking VEGFR-3 suppresses angiogenic sprouting and vascular network formation. *Nature* **454,** 656–660 (2008).
35. Isogai, S., Lawson, N. D., Torrealday, S., Horiguchi, M. & Weinstein, B. M. Angiogenic network formation in the developing vertebrate trunk. *Development* **130,** 5281–5290 (2003).
36. Lu, P. F., Ewald, A. J., Martin, G. R. & Werb, Z. Genetic mosaic analysis reveals FGF receptor 2 function in terminal end buds during mammary gland branching morphogenesis. *Dev. Biol.* **321,** 77–87 (2008).
37. Chi, X. *et al.* Ret-dependent cell rearrangements in the wolffian duct epithelium initiate ureteric bud morphogenesis. *Dev. Cell* **17,** 199–209 (2009).

DOI: 10.1038/ncb2103

METHODS

Mouse embryonic stem cells. R1 wild-type, YFP-expressing wild-type (hybrid of two 129 sub-strains)[38], mouse strains expressing DsRed-MST and Z/red[39] (129S6B6-F1 hybrid embryonic stem cell line designated G4), and *Vegfr2*$^{+/lacz}$- and *Vegfr2*$^{-/-}$-embryonic stem cells[40], were gifts from A. Nagy and J. Rossant (Samuel Lunenfeld Research Institute, Canada). *Vegfr2*$^{+/egfp}$ embryonic stem cells were generated by targeted insertion of *egfp* into exon 1 in the *Vegfr2* locus in E14 embryonic stem cells (strain 129/Ola)[41]. *Vegfr1*$^{+/lacz}$ embryonic stem cells[10] were provided by G. H. Fong (University of Connecticut Health Center, USA). *Dll4*$^{+/lacz}$-, *Dll4*$^{lacz/lacz}$- and *Nrarp*$^{+/lacz}$-embryonic stem cells were from Regeneron Pharmaceuticals.

Embryoid bodies. embryonic stem cells were cultured, and embryoid bodies were generated, as previously described[42]. Briefly, embryonic stem cells were routinely cultured on a layer of irradiated mouse embryonic fibroblasts (DR4) in the presence of leukaemia inhibitory factor (LIF). For experiments, cells were cultured for two passages without feeders, then trypsinized, depleted of LIF, mixed with another strain in case of competition and left in suspension as hanging drops (day 0). On day four the formed embryoid bodies were transferred to a polymerized collagen I gel (as previously described[42]) with addition of 30 ng ml^{-1} VEGFA164 (Peprotech). Medium with or without VEGFA164, DMSO or DAPT (all at concentrations of 5 μM; Sigma-Aldrich, LY-374973) was changed on day six and every day thereafter.

Time-lapse laser scanning microscopy. Embryoid bodies were cultured in collagen I in 24-well plates (Mattek). On day six, or as indicated, the plate was transferred to a LSM Pascal version 4.2 microscope system (Zeiss; equipped with a motorized stage, incubator S-M and POC-R cultivation system) maintained at 37 °C and 5% CO_2 with a humidifier. *Z*-slices were acquired (5–9 per field every 20 min using 2% laser capacity). Medium was changed every day until termination. Up to 16 different wells were imaged per experiment using Multi time series version 4.0.12. Cellular migration was measured using Imaris software.

Image segmentation and quantitative cell-tracking analysis. Time-lapse laser scanning confocal microscopy images of chimaeric embryoid bodies from different embryonic stem populations were analyzed using Bitplane Imaris 7.0.0. Images were segmented using surface mode selecting for DsRed, eGFP or YFP channels and adjusting thresholds accordingly. Single cells tracks were selected manually and track information was collected for migration directionality and average speed. Approximately 4–6 cells in 3–5 experiments were measured for each genetic background, with the exception of YFP(wild-type) fibroblasts where only 2 experiments were used for quantification.

Migration directionality was assessed using the track straightness function in Imaris software that consists of the ratio between track displacement length (distance between first and last surface's position) and track length (total length of displacements within the track).

Average speed was assessed using the average track speed function in Imaris software and is calculated by the track length divided by the time between first and last object in the track, and is expressed in μm s^{-1}. Collected data were statistically analyzed using GraphPad Prism 5.0 software.

Immunostaining/western blotting of embryoid body material. Embryoid bodies in collagen I gels were processed for whole-mount immunohistochemical staining as described previously[42]. The following primary antibodies were used for detection: rat anti-mouse CD31 antibody (1:1,000; PharMingen, 55773), goat anti-mouse VEGFR-2 (1:200; R&D, AF644), goat anti-mouse Dll4 (1:200; R&D, AF1389) and rabbit anti-actin (1:5,000; Sigma-Aldrich, A5060). Secondary antibodies: Alexa 568 goat anti-rat IgG (1:500), Alexa 488 goat anti-rat IgG (1:500), Alexa 555 donkey anti-goat IgG (1:500), Alexa 488 donkey anti-rabbit (1:500; Molecular Probes), Cy5 donkey anti-rabbit IgG (1:500; Jackson ImmunoResearch), and horse radish peroxidase (HRP)-conjugated anti-rabbit IgG and HRP-conjugated rabbit anti-goat IgG (1:8,000; Dako). Hoechst 33342 was used to visualize the nuclei. Total embryoid body cell lysates were prepared as previously described[42]. Protein concentration was measured using BCA (bicinchoninic acid) protein assay (Pierce). Equal amounts of proteins were separated on NuPAGE 4–12% MOPS gel (Invitrogen) and transferred on PVDF (polyvinylidene fluoride) membrane (GE Healthcare Biosciences).

Flow cytometry. Embryoid bodies in collagen (approximately 700) were dissociated by treatment with 2.5 mg ml^{-1} Collagenase A (Roche, 10103578001) in complete embryoid-body media (Dulbecco's modified Eagle's medium/glutamax, GibcoBRL, 61965-026; 20% (v/v) FBS; fetal bovine serum; Sigma, F-7524; 25 mM HEPES buffer, GibcoBRL, 15630-056; 1.2 mM sodium pyruvate, GibcoBRL, 11360-039 and 19 mM monothioglycerol, Sigma, M-6145), for 40 min at 37 °C. The Collagenase A solution was replaced with 10 ml cold FACS buffer (PBSA; PBS with 0·01% (v/v) sodium azide; 2 mM EDTA and 0.5% (v/v) BSA, Sigma, A4378), the embryoid bodies were passed through a 70 μm cell strainer (BD, 352350) and were washed with 10 ml cold FACS buffer. The cell suspension was further passed through a 35 μm cell strainer (BD, 352235) and cells were stained with biotinylated PECAM-1 (BD Pharmingen, 553371), streptavidin Alexa Fluor 633 (Invitrogen, S21375) or streptavidin Phycoerythrin (PE)–Cy7 (1:200; eBioscience, 25-4317-82) and an anti-mouse CD16/CD32 Fc block (BD Pharmingen, 553142), all diluted 1:200 in FACS buffer and incubated for 30 min at 4 °C. FACS was performed using a cytomation MoFlo cytometer. Data were subsequently analysed with FlowJo v8.7.1.

Quantitative PCR. RNA from embryoid bodies in collagen at day 10 was extracted and purified using RNAeasy-kit (Qiagen). RNA concentrations were measured and adjusted equally, followed by reverse transcription by SuperScript III (Invitrogen). Quantitative PCR with Taqman probes for *Dll4* (Mm00444619), *Cd31* (Mm01242584), *Vegfr1* (Mm00438980), *Vegfr2* (Mm00440099) and *Hey1* (Mn00468865_m1) was run in an Applied Biosystems 7900HT real-time thermal cycler. The expression levels were normalised to internal β-actin (4852341E).

Statistical analysis. Statistical analysis was performed with Prism 5 software (GraphPad) using two-, or one-tailed, unpaired *t*-tests. When variances were significantly different between two samples an unpaired *t*-test with Welch's correction was applied.

Animal Procedures. The following mice were used as hosts: C57BL/6JCrl (Charles River Laboratories International, USA), C57BL/6-Tg(CAG-eGFP)1Osb/J[43] and Tg(CAG-DsRed-MST)Nagy/J (Jackson Laboratory, USA)[39].

Retina analysis. Retinas were fixed, isolated and labelled using isolectin B4 directly conjugated to Alexa 488, 568 or 647 (Invitrogen) and flatmounted and imaged as described previously[2]. EdU was injected intraperitoneally 4 h before tissue harvesting and detection through Click-iT chemistry, performed according to manufacturer's instructions (Click-iT imaging kit, Invitrogen).

Zebrafish intravital imaging. The transgenic zebrafish lines used were *Tg(kdrl:eGFP)*[44], denoted as *kdrl:eGFP;* Tg(*kdrl:mCherry)*[45], denoted as *kdrl:mCherry; Tg(fli1a:eGFP)*, denoted as *flia:eGFP*; *Tg(fli1a:NLS–GFP)*[46], denoted as *fli1a:NLS–GFP;* and intercrosses. Embryos and fish were maintained in the Hubrecht Institute or the Cancer Research UK London Research Institute under standard husbandry conditions.

For images in Figure 5g–j, MS-222 anesthetized embryos were mounted approximately 48 h post-fertilization in E3 medium containing 0.5% (w/v) low-melting-point agarose (Invitrogen) on a culture dish with a glass cover slip replacing the bottom. Pigment formation was blocked by the addition of PTU (propylthiouracil) 24 h post-fertilization onwards. Confocal image stacks were collected on an SP5 confocal microscope (Leica Microsystems) using a ×20 dry objective (N.A. 0.7). eGFP excitation was with 488 nm and mCherry excitation was with 561 nm laser light. Images were processed using ImageJ software (http://rsbweb.nih.gov/ij).

For images in Figure 7k–n, *fli1a:eGFP* embryos were injected at the 1–2 cell stage with 40 pg *pTol2-kdrl:dTomato* plasmid DNA and 100 pg of *in vitro* synthesized (SP6 mMessage mMachine kit, Ambion) *Tol2* mRNA. At approximately 28 h post-fertilization MS-222 anesthetized embryos were mounted in 0.8% (w/v) low-melting-point agarose, and a time series of confocal *z*-stacks were collected on a Zeiss LSM-710 confocal microscope with a ×20 water-immersion dipping objective (N.A. 1.0). Images were processed using the Imaris software package.

Molecular Biology. To generate *pTol2-kdrl:dTomato* plasmid the zebrafish *kdrl* promoter [44], coding sequence for the dTomato red fluorescent protein[47] and an SV40 poly(A) signal were inserted into the Tol2 plasmid[48].

Retina quantifications. Complete high resolution three-dimensional (3D) rendering of whole mount retinas and embryoid bodies were acquired using a Laser Scanning Microscope Pascal version 4.2 microscope system (Zeiss), equipped with a motorized stage. Up to four channels from up to 150 positions in the *x*- and *y*-planes and 9 slices in the *z* plane, acquired with either a ×40 or ×20 lens, were stitched together using the Multi time series software, version 4.0.12. In the embryoid bodies, 50–200 tip cells were manually scored and marked for genotypic origin using the LSM image browser (Zeiss). Tiled stacks of whole retinas were analysed with Volocity 5.1.1. Tip regions were defined as the regions from the very tips to the second or third vascular loop (see Supplementary Information, Fig. S4). The threshold of intensity to detect the 3D endothelium was set by eye for each retina. A similar strategy was used to detect the respective fluorophore. The intersecting voxels were recorded and contribution of the respective cell type was calculated as the ratio between the intersecting volume and the total volume of the endothelium. Data were acquired from complete retinas, each divided into ten regions to correlate contribution between areas to each other.

38. Nagy, A., Rossant, J., Nagy, R., Abramow-Newerly, W. & Roder, J. C. Derivation of completely cell culture-derived mice from early-passage embryonic stem cells. *Proc. Natl Acad. Sci. USA* **90,** 8424–8428 (1993).
39. Vintersten, K. *et al.* Mouse in red: red fluorescent protein expression in mouse ES cells, embryos and adult animals. *Genesis* **40,** 241–246 (2004).
40. Shalaby, F. *et al.* Failure of blood-island formation and vasculogenesis in Flk-1-deficient mice. *Nature* **376,** 62–66 (1995).
41. Hooper, M., Hardy, K., Handyside, A., Hunter, S. & Monk, M. HPRT-deficient (Lesch-Nyhan) mouse embryos derived from germline colonization by cultured cells. *Nature* **326,** 292–295 (1987).
42. Jakobsson, L. *et al.* Heparan sulfate in trans potentiates VEGFR-mediated angiogenesis. *Dev. Cell* **10,** 625–634 (2006).
43. Okabe, M., Ikawa, M., Kominami, K., Nakanishi, T. & Nishimune, Y. 'Green mice' as a source of ubiquitous green cells. *FEBS Lett.* **407,** 313–319 (1997).
44. Jin, S. W., Beis, D., Mitchell, T., Chen, J. N. & Stainier, D. Y. Cellular and molecular analyses of vascular tube and lumen formation in zebrafish. *Development* **132,** 5199–5209 (2005).
45. Hogan, B. M. *et al.* Ccbe1 is required for embryonic lymphangiogenesis and venous sprouting. *Nat. Genet.* **41,** 396–398 (2009).
46. Lawson, N. D. & Weinstein, B. M. *In vivo* imaging of embryonic vascular development using transgenic zebrafish. *Dev. Biol.* **248,** 307–318 (2002).
47. Shaner, N. C. *et al.* Improved monomeric red, orange and yellow fluorescent proteins derived from *Discosoma* sp. red fluorescent protein. *Nat. Biotechnol.* **22,** 1567–1572 (2004).
48. Urasaki, A., Morvan, G. & Kawakami, K. Functional dissection of the Tol2 transposable element identified the minimal cis-sequence and a highly repetitive sequence in the subterminal region essential for transposition. *Genetics* **174,** 639–649 (2006).

nature cell biology

DOI: 10.1038/ncb2103

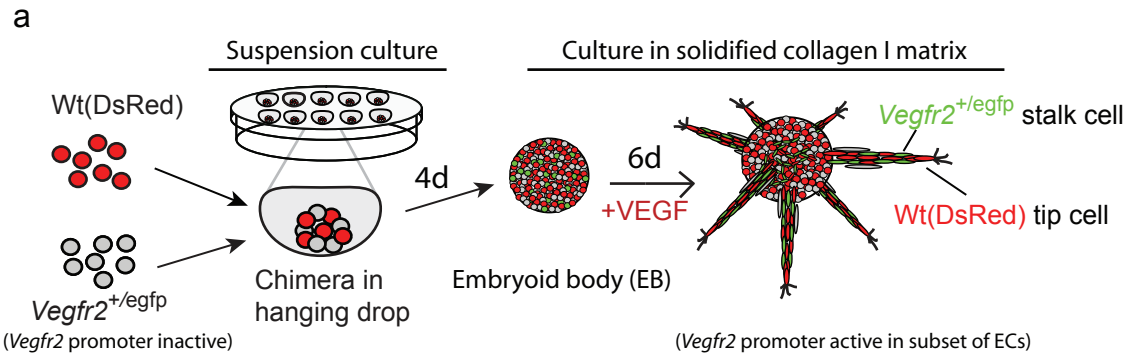

Figure S1 (**a**) Generation of chimeric sprouting vasculature from differentiating ES cells. Traceable ES cells with disparate genetic composition are mixed in suspension. Four days after differentiation the EBs are cultured in a solidified collagen I matrix and respond to exogenous VEGFA164 by sprouting angiogenesis.

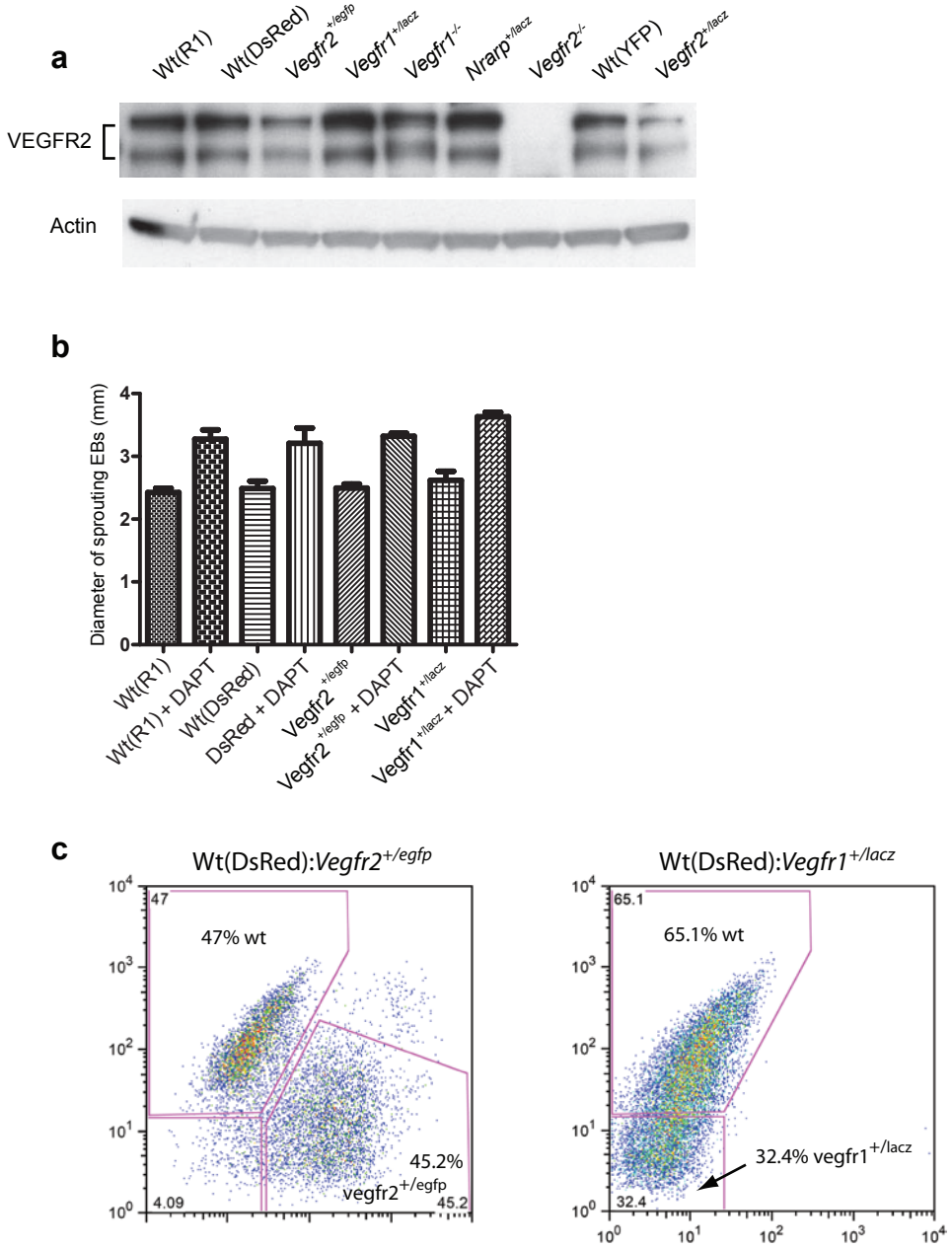

Figure S2 (**a**) VEGFR2 levels in total cell lysates from d10 EBs of indicated genotype. VEGFR2 is reduced in *Vegfr2*$^{+/egfp}$ and *Vegfr2*$^{+/lacz}$ EBs compared to the various Wt cells (R1, DsRed, eYFP). Actin serves as a loading control. **b**, Diameter of the total sprouting region in EBs measured from one side of the extending vascular front to the other. There is no difference in sprouting abilities between the various cell lines but DAPT treatment increases the sprouting diameter (P=0.0002 for R1 with/without DAPT) for all genotypes. **c**, Sorted single ECs from chimeras as indicated. In DsRed:*Vegfr2*$^{+/egfp}$ chimeras 47% of the ECs are of DsRed genotype and 45.2 of *Vegfr2*$^{+/egfp}$ origin. In DsRed:*Vegfr1*$^{+/lacz}$ chimeras 65% of ECs are of DsRed genotype whereas 32.4 are from *Vegfr1*$^{+/lacz}$.

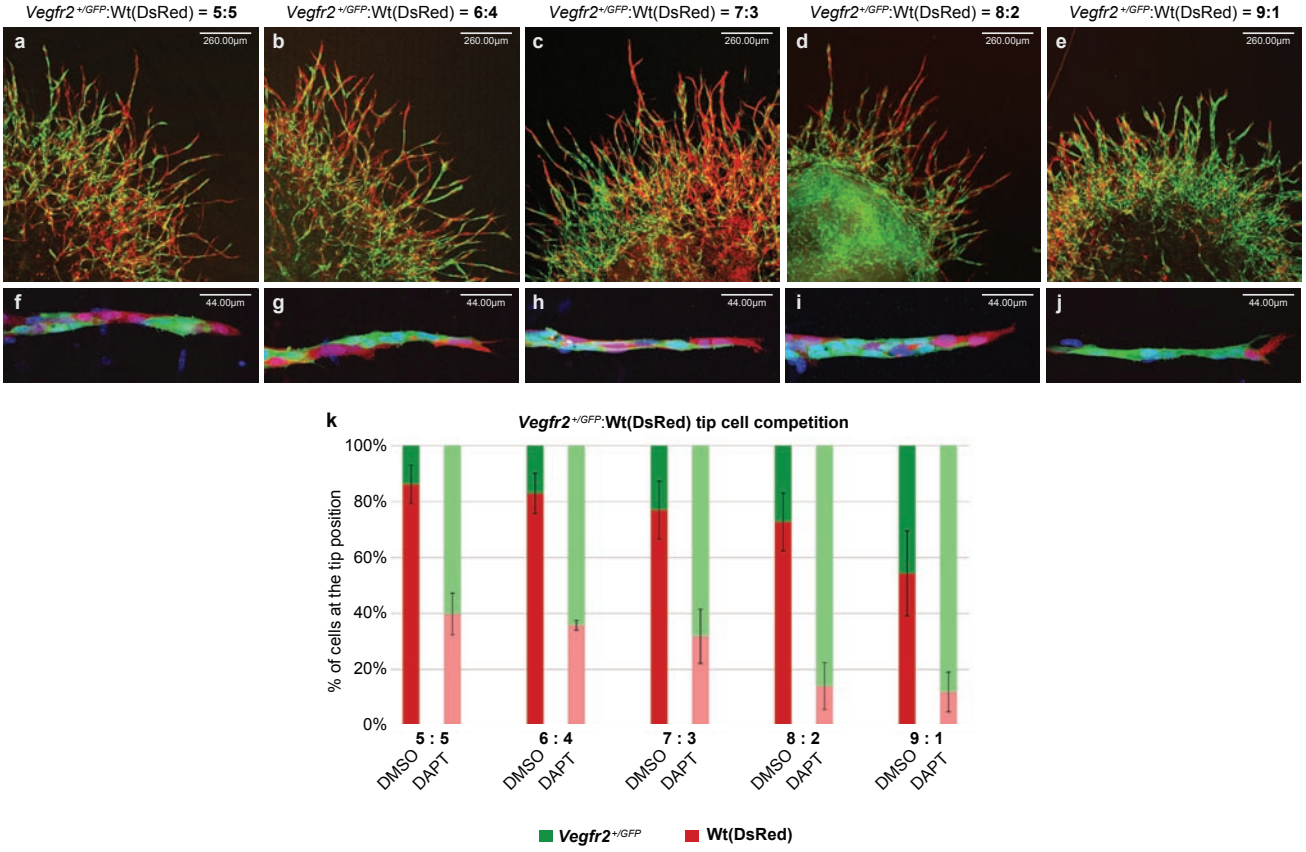

Figure 3 Chimeric EBs derived from different ES cell strains develops a mosaic vasculature. Wt cells with ubiquitous expression of DsRed compete with increasing amounts of *Vegfr2*$^{+/egfp}$ cells for the tip position in 10 day EBs. (**a-e**) Clones with reduced VEGFR2 avoid the tip position. The overall amount of VEGFR2 cells (green) increases according to rising cell numbers. Wt cells (red), even when underrepresented in numbers of cells, mainly occupied the tip position. (**f-j**) Wt cells have an advantage to reach the tip position. Visualisation of single sprouts shows decreased numbers of Wt cells within the sprout according to increased amounts of VEGFR2 cells, but the tip position is still occupied by Wt cells. (**k**) Quantification of tip cell contribution. Approximately 85% of tip cells are derived from Wt cells in a 5:5 chimeric situation with *Vegfr2*$^{+/egfp}$ cells. The percentage of Wt cells occupying the tip position gradually decreases to 50% in a situation where only one tenth of cells in the EB are Wt. Treatment with 5 µM DAPT abrogates the advantage of Wt for the tip position, leading to tip cell levels according to the amount of initiated cell numbers.

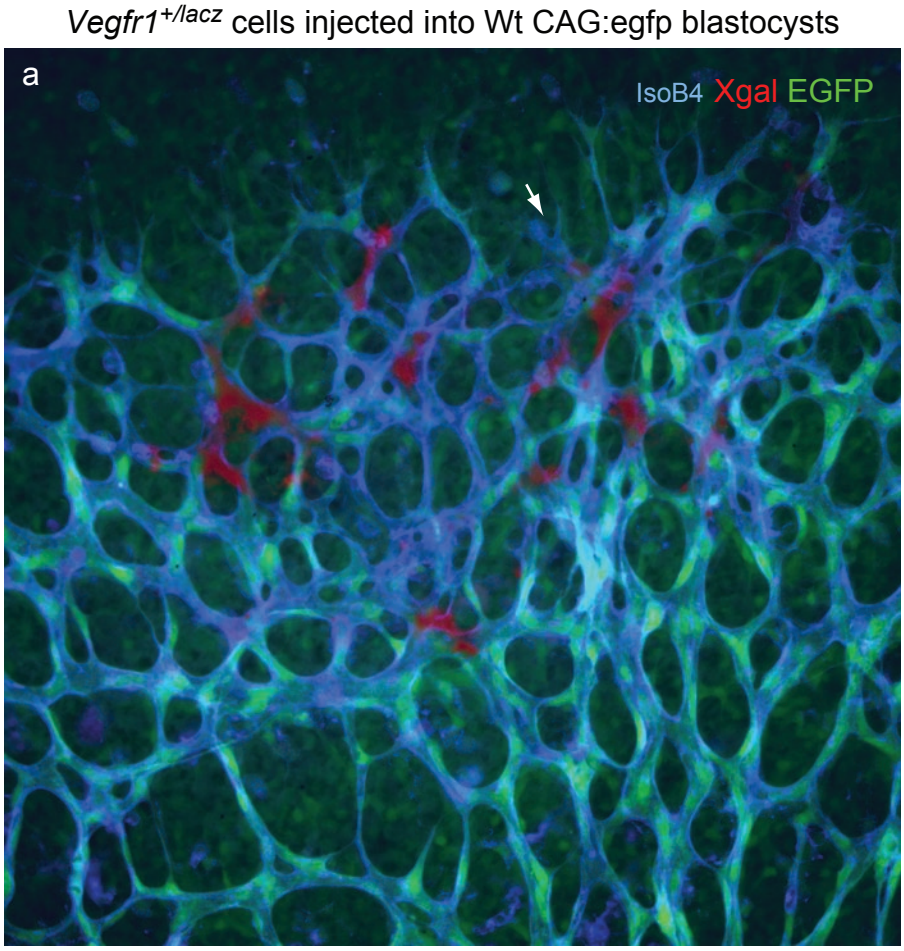

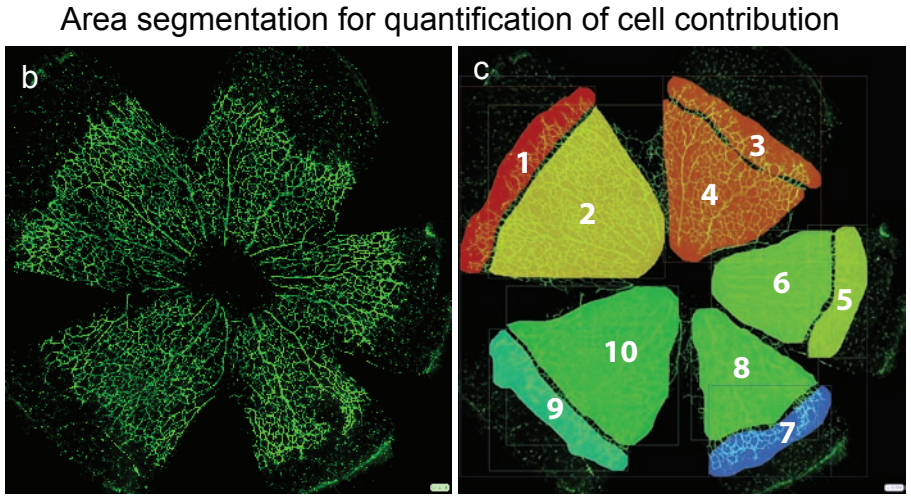

Figure S4 a, example of chimeric *Vegfr1*$^{+/lacz}$/CAG:egfp retina. *Vegfr1*$^{+/lacz}$ cells (X-gal, red) contribute to the periphery of retinal vessels. Note that although only two or three of the X-gal positive *Vegfr1* heterozygous cells are at the very front, none of the *Vegfr1*$^{+/lacz}$ cells are found in the central region of the retina. Arrow indicates an X-gal negative *Vegfr1*$^{+/lacz}$ cell identified by the absence of host-derived GFP expression. **b, c,** Illustration of areas used in quantification of genotypic cell contribution to tip or stalk regions in chimeric retinas. Areas are compared in sets of pairs; 1 with 2, 3 with 4 etc.

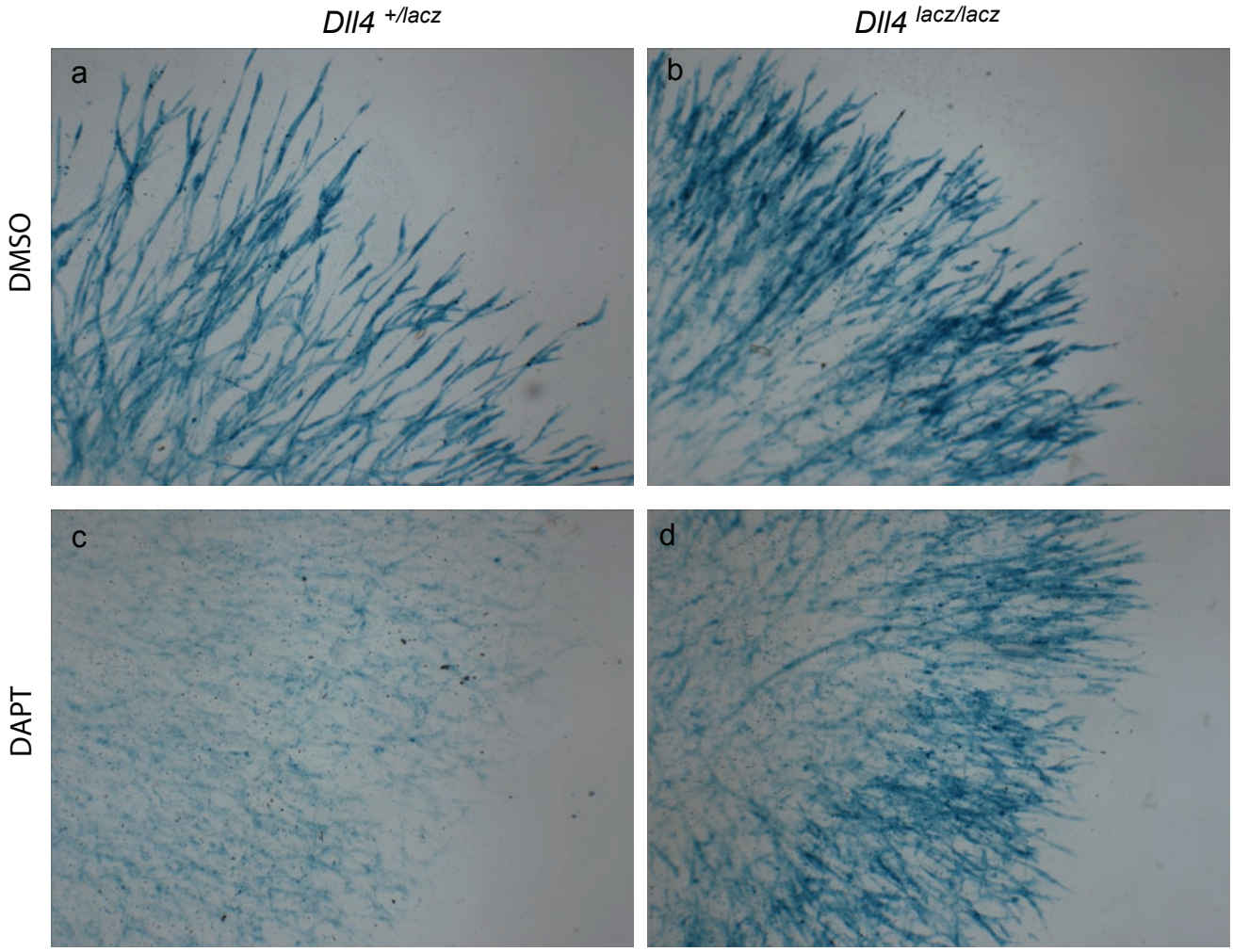

Figure S5 Overview transmitted light images of EBs derived from *Dll4*$^{+/lacz}$ (**a, c**) and *Dll4*$^{lacz/lacz}$ (**b, d**) ES cells. X-gal staining (blue) illustrates strong Dll4 promoter activity in the sprouts, especially towards the distal tip. DAPT treatment (**c, d**) consistently reduced X-gal staining, suggesting that full Dll4 activity requires Notch signalling.

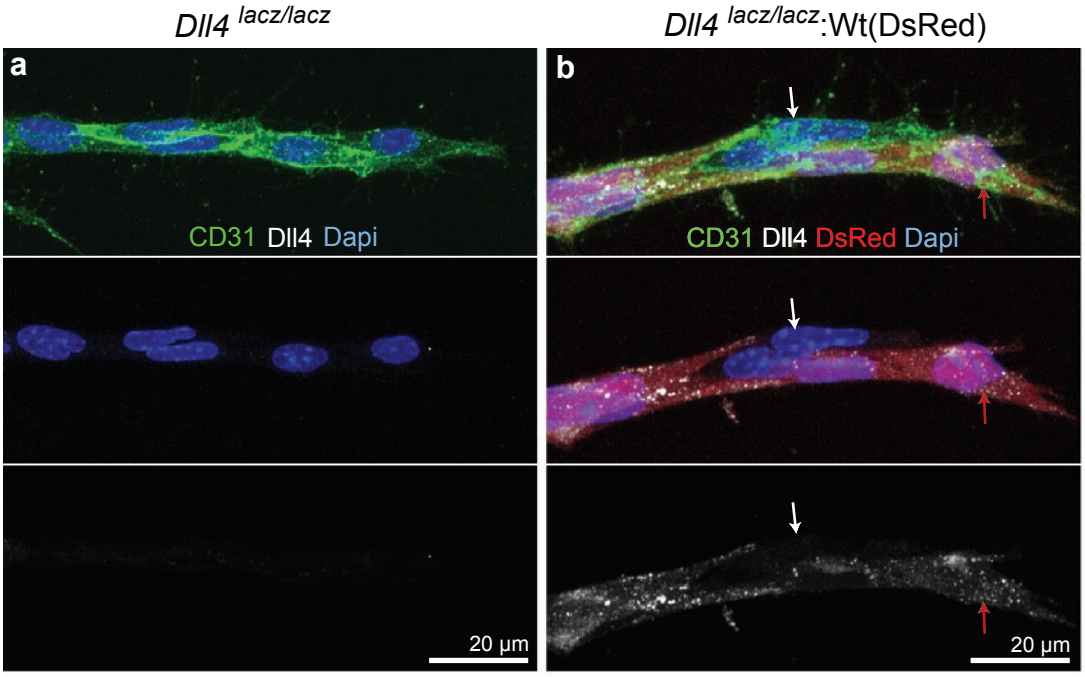

Figure S6 Confocal micrograph of sprouts in *Dll4*$^{lacz/lacz}$ EBs (**a**) and in chimeric DsRed:*Dll4*$^{lacz/lacz}$ EBs (**b**). CD31 labelling (green) outlines endothelial cells, nuclei are labelled with Dapi (blue). Dll4 antibody labelling (greyscale) is abundant in Wt (DsRed) cells (red arrows in **b**), but absent in Dll4 deficient (*Dll4*$^{lacz/lacz}$) ES cells (**a**, white arrows in **b**).

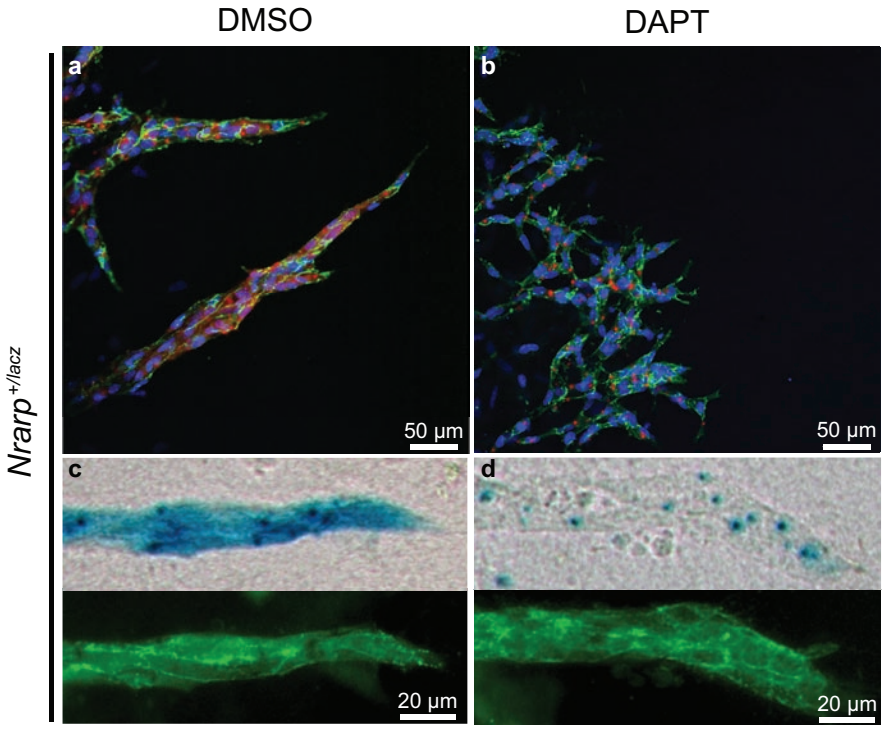

Figure S7 Expression of the Notch target gene Nrarp in *Nrarp*$^{+/lacz}$ EBs is strongly inhibited by DAPT treatment. (**a**) X-gal staining revealed by fluorescence (red) illustrates strong expression in control (DMSO) treated EBs, specifically in endothelial cells (highlighted by VE-cadherin labelling, green). (**b**) DAPT treated EBs show residual Xgal positive dots, but lack most of the cytoplasmic Xgal staining. (**c, d**) Transmitted light (top) and VE-cadherin counterstaining (bottom) images of DMSO and DAPT treated *Nrarp*$^{+/lacz}$ sprouts.

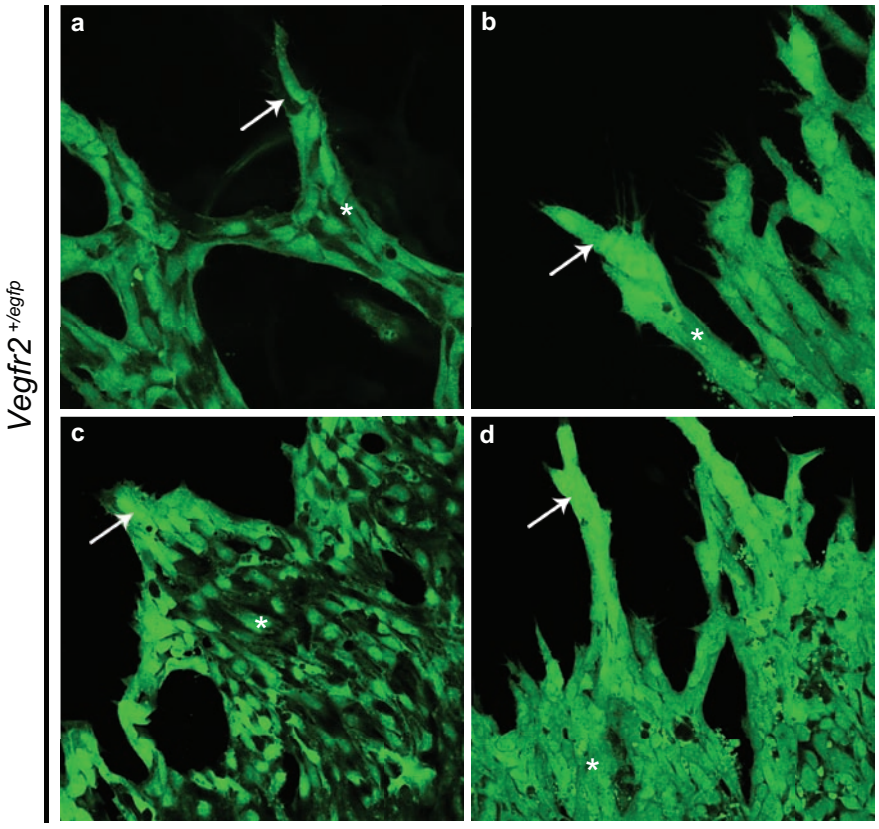

Figure S8 (**a-d**) GFP expression in *Vegfr2*$^{+/egfp}$ EBs (green, arrows). The eGFP signal in control sprouts is abundant in the cytoplasm and nucleus of cells in the tip region of the sprout. Cells further back show markedly reduced cytoplasmic eGFP, and various levels of nuclear retained signal. Upon DAPT treatment, all ECs throughout the EB show intense cytoplasmic and nuclear eGFP signal, indicating constant high level production of eGFP, and hence high VEGFR2 promoter activity.

Supplementary Movie Legends

Movie 1 Cell shuffling in Wt (DsRed):*Vegfr2*$^{+/egfp}$ sprouting EB. Time lapse confocal laser scanning microscopy of Wt (DsRed):*Vegfr2*$^{+/egfp}$ EB chimera treated with 30 ng ml^{-1} VEGFA. Cell shuffling in the stalk region as well as in the tip position is observed throughout the acquisition period. *Vegfr2*$^{+/egfp}$ cells are hardly found as tip cells, and when they reach the tip position the cells are rapidly replaced.

Movie 2 Cell shuffling in Wt (DsRed):*Vegfr2*$^{+/egfp}$ sprouting EB under DAPT treatment. Time lapse confocal laser scanning microscopy of Wt (DsRed):*Vegfr2*$^{+/egfp}$ EB chimera treated with 30 ng ml^{-1} VEGFA with DAPT. Cell shuffling in the stalk region as well as in the tip position is observed throughout the acquisition period. Note that *Vegfr2*$^{+/egfp}$ frequently gain and regain the tip position when Notch signaling is inactive (compare with supplementary video 1).

Movie 3 Example of single-cell tracking on EBs. Surface-rendering of a single YFP-positive cell (light blue) and of a single DsRed-positive cell (light yellow) from a time lapse confocal laser scanning microscopy of Wt(eYFP):Wt(DsRed) EB chimera treated with 30 ng ml^{-1} VEGFA.

Movie 4 Tip cell competition in Wt(eYFP):Wt(DsRed) EBs. Time lapse confocal laser scanning microscopy of Wt(eYFP):Wt(DsRed) EB chimera treated with 30 ng ml^{-1} VEGFA. Note, that both Wt cells can equally challenge the tip cell.

Movie 5 Tip cell competition in Wt(DsRed):*Vegfr2*$^{+/egfp}$ EBs. Time lapse confocal laser scanning microscopy of Wt(DsRed):*Vegfr2*$^{+/egfp}$ EB chimera treated with 30 ng ml^{-1} VEGFA. Note that *Vegfr2*$^{+/egfp}$ cell can reach the tip position, but it is rapidly replaced by a Wt endothelial cell.

Movie 6 Tip cell competition in Wt(eYFP):Wt(DsRed):*Vegfr1*$^{+/lacz}$ EBs. Time lapse confocal laser scanning microscopy of triple chimeric Wt(eYFP):Wt(DsRed):*Vegfr1*$^{+/lacz}$ EB treated with 30 ng ml^{-1} VEGFA. Note that *Vegfr1*$^{+/lacz}$ cell stays a longer time as tip cell than Wt cells (compare with supplementary video 4).

Movie 7 *In vivo* tip cell competition in Tg(kdrl:mCherry, fli1:NLS-eGFP) zebrafish 1. Timelapse recording of the angiogenic sprouting in double transgenic Tg(kdrl:mCherry, fli1:NLS-eGFP) embryos enable simultaneous monitoring of filopodial behavior (kdrl:mCherry) and positioning of the cell body (fli1:NLS-eGFP). White arrows indicate the cell initially taking the tip cell position (with green arrow marking its filopodia); purple arrows indicate cells taking over the tip cell position at later stages. The yellow arrow marks a second cell moving past the original tip cell. Images were recorded every 25 min.

Movie 8 *In vivo* tip cell competition in Tg(kdrl:mCherry, fli1:NLS-eGFP) zebrafish 2. Time lapse confocal laser scanning microscopy of double transgenic Tg(*kdrl:mCherry*, *fli1:NLS-eGFP*) zebrafish embryos. First two white arrows indicate two cells shuffling back and forth. White arrow in new sprout indicates initial leader, purple arrow indicates cell taking over the tip cell position at later stages. The yellow arrow marks a second cell moving past the original tip cell while the first cell moves all the way to the base of the sprout. Images were recorded every 25 min.

Movie 9 *In vivo* tip cell battling between a kdrl:dTomato cell and a fli:GFP cell in zebrafish. Time lapse confocal laser scanning microscopy of *kdrl:dTomato* labeled endothelial cell in a *fli:GFP* zebrafish embryo. The red cell and a green cell compete for the tip position. Images were captured every 15min.

Movie 10 *In silico* simulation of VR1:Wt chimera. Movie represents 24hrs of real time in a sprout comprising 50% HT cells. HT cells (green) Wt (red), VR2 receptor levels are indicated by low to high intensity of the cells colour. Movie shows HT cells overtake the head tip cell frequently whereas it takes a long time before a Wt cell overtakes. Note the cyclic self-organization of the sprout between fully segregated and then well-mixed arrangements of the two cell types.

Movie 11 *In silico* simulation of VR2:Wt chimera. Movie represents 24hrs of real time in a sprout comprising 50% HT cells. HT cells (green) Wt (red), VR2 receptor levels are indicated by low to high intensity of the cells color. Movie shows Wt cells quickly overtake the head tip cell. The cyclic self organization of the sprout between fully segregated and then well mixed arrangements of the two cell types also occurs in the VR2 chimera.

Detailed shuffling sprout model

The same model was used with only simple adjustments to represent the dynamics of tip cell selection and shuffling of cells within a migrating sprout.

To let the row of ECs in the model now represent a single growing sprout, as studied in the *in vitro* sprouting assay, a number of changes were made to the initial set up of the vessel and environment. The left and right ends of the vessel were detached (periodic boundary conditions were no longer used), in order to have it instead represent a directed sprout growing in the right hand direction. The cell furthest right, leading the sprout was referred to as the 'head tip' leading the sprout forward, distinguishing it from other 'tip cells' in the sprout, defined by the model as having over half the maximum VEGFR2 level and at least1.2 x initial memAgent numbers, i.e. some filopodia have developed. 30 microns of VEGF environment was placed above, below and to the right of the sprout. The cell furthest right was biased to become a tip cell by both its increased surface area exposed to VEGF and its lack of a neighbour cell ahead of it, thus it only experiences half the neighbourly inhibition of the other cells. To avoid biasing the cell furthest left however, which would be connected to cells further back in the sprout, the protein levels it experienced from the cell to its right were simply doubled, and the proteins levels it presents to this cell on its single junction are halved, as the other half would have been directed to the junction with the unseen neighbour on its left.

Shuffling of cells past each other was only allowed to occur once a salt and pepper pattern, consisting of no adjacent tip cells, had been stable for 100 time steps. In order to

model the shuffling of cells simply, each cell was given a probability of shuffling up towards to the head tip position. If on a given time step the probability allows it to shuffle, the cell simply swaps places with the cell to its right, i.e. all the cell's memAgents including those in filopodia are shifted right by one cell length, 20 grid sites, and similarly all of the neighbour cell's memAgents are shifted left by one cell length. All cells except the actual head tip cell try to shuffle every time step. If the cell neighbouring the head tip overtakes the head tip, and the head tip has filopodia projecting out horizontally, such that upon swapping position they would overlap with the new overtaking cell, then these filopodia are instantly retracted.

1.1 Shuffling Probability

1.1.1 Fixed Function

Initially, in a sprout comprised only of Wt cells, a fixed probability for any tip cell to overtake was used in order to find the value at which a similar duration could be gained for head tips to maintain their position before being overtaken to that measured *in vitro* (approximately 3.5 hours). It was found that if $P(shuffling) = 0.01$, per time step (representing 15 seconds), given the cell classifies as a tip cell, achieved the closest WT duration. This value was then used as a guide in order to design the active Notch and active VR2 based function for use in testing chimera head tip durations.

1.1.2 Active Notch Shuffling Function

It was hypothesized that the active Notch levels of the cells may be involved in determining the shuffling rate of cells. A simple function was devised to test this as follows:

$P(shuffling) = a - bN'$,

Where N' is the active Notch level of the cell, a was set to 0.015 and b was set to 5×10^{-5}. This gave values that centered around 0.01, the fixed value define above, but allowed a reasonable range of probabilities by scaling the possible active Notch levels. The stipulation that cells must be defined as tip cells in order to shuffle was no longer used, as the active Notch function inherently selects tip cells as more likely to shuffle.

This function was validated against the original model results to check that the percentage of HT head tip cells at a given time step still matched in vitro results. At 10,000 time steps (41hrs) the cell type at the head tip was recorded and results averaged over 50 runs to see which cell type was more likely to lead the sprout (Fig 6c).

1.1.3 Active VEGFR-2 Shuffling Function

Further, we wanted to compare the above with simulations using a different shuffling function. It is plausible that shuffling could be regulated directly via the VEGFR-2 receptor as it is known to regulate endothelial cell migration.

The probability of Cell A overtaking cell B, to its right, is given by:

$P(shuffling) = c(V'_A - (kV'_B))$,

where V'_A and V'_B are the active VEGFR-2 receptor level of the given cells. Constants c and k were set to 0.25 and 0.3 respectively, again calibrated to give approximately the P(shuffling) = 0.01, found to give matching durations in the WT only sprout.

Again at 10,000 time steps (41hrs) the cell type at the head tip was recorded and results averaged over 50 runs to see which cell type was more likely to lead the sprout (Fig. 6d). This function cannot match the *in vitro* results (shown in Fig. 6b) that DAPT treatment returns the percentage of HT head tip cells to approximately 50% in both the VR1 and VR2 chimeras. DAPT treatment was simulated by turning off the Notch activation function in each cell.